3-Aryl/Heteroaryl-5-amino-1-(3′,4′,5′-trimethoxybenzoyl)-1,2,4-triazoles as antimicrotubule agents. Design, synthesis, antiproliferative activity and inhibition of tubulin polymerization

Romeo Romagnoli[a,∗], Filippo Prencipe[a], Paola Oliva[a], Stefania Baraldi[a], Pier Giovanni Baraldi[a], Andrea Brancale[b], Salvatore Ferla[b], Ernest Hamel[c], Roberta Bortolozzi[d], Giampietro Viola[d,∗]

[a] *Dipartimento di Scienze Chimiche e Farmaceutiche, Università di Ferrara, 44121 Ferrara, Italy*
[b] *School of Pharmacy and Pharmaceutical Sciences, Cardiff University, King Edward VII Avenue, Cardiff CF10 3NB, UK*
[c] *Screening Technologies Branch, Developmental Therapeutics Program, Division of Cancer Treatment and Diagnosis, Frederick National Laboratory for Cancer Research, National Cancer Institute, National Institutes of Health, Frederick, MD 21702, USA*
[d] *Dipartimento di Salute della Donna e del Bambino, Laboratorio di Oncoematologia, Università di Padova, 35131 Padova, Italy*

ARTICLE INFO

ABSTRACT

Many natural and synthetic substances are known to interfere with the dynamic assembly of tubulin, preventing the formation of microtubules. In our search for potent and selective antitumor agents, a novel series of 1-(3′,4′,5′-trimethoxybenzoyl)-5-amino-1,2,4-triazoles were synthesized. The compounds had different heterocycles, including thiophene, furan or the three isomeric pyridines, and they possessed a phenyl ring bearing electron-releasing or electron-withdrawing substituents at the 3-position of the 5-amino-1,2,4-triazole system. Most of the twenty-two tested compounds showed moderate to potent antiproliferative activities against a panel of solid tumor and leukemic cell lines, with four (**5j**, **5k**, **5o** and **5p**) showing strong antiproliferative activity ($IC_{50} < 1\,\mu M$) against selected cancer cells. Among them, several molecules preferentially inhibited the proliferation of leukemic cell lines, showing IC_{50} values 2-100-fold lower for Jurkat and RS4;11 cells than those for the three lines derived from solid tumors (HeLa, HT-29 and MCF-7 cells). Compound **5k** strongly inhibited tubulin assembly, with an IC_{50} value of $0.66\,\mu M$, half that obtained in simultaneous experiments with CA-4 ($IC_{50} = 1.3\,\mu M$).

1. Introduction

The microtubule system of eukaryotic cells, a protein system composed of αβ-tubulin heterodimers in a dynamic equilibrium with microtubules, is a critical element in a variety of fundamental cellular processes, including mitosis and cell division, determination and maintenance of cell shape, organization of intracellular architecture, secretion, intracellular transport and regulation of motility [1–3]. Given their significant role in the cellular functions that are critical to the life cycle of the cell, microtubules are a proven molecular target for cancer chemotherapeutic agents and continue to receive substantial attention for development of new and improved drugs [4–6].

Among the distinct classes of tubulin-binding agents that have been identified on the basis of their different mechanisms of action and binding sites on tubulin, two groups are of particular importance in the clinical treatment of cancer [7,8]. First are the vinca alkaloid microtubule-destabilizers, typified by vinblastine, vincristine, vinorelbine and vinflunine. Second are the taxoids, paclitaxel (Taxol), docetaxel (Taxotere) and cabazitaxel (Javetana). These compounds act with an opposite effect, interfering with microtubule disassembly and stabilizing the microtubule structure. These drugs are used to treat a broad range of leukemias and lymphomas as well as many types of solid tumors [9–11]. Nevertheless, the clinical success of these two classes of compounds has stimulated intensive research aimed at discovering additional microtubule-targeting drugs with clinical potential [12].

A third class of note, due to the discovery of numerous natural products and synthetic compounds that target this site, are agents that bind in the colchicine site [13,14]. Such compounds inhibit the polymerization of tubulin into microtubules and display wide structural heterogeneity [15,16]. One of the most notable of these compounds, both for its potency and structural simplicity is the naturally occurring *cis*-stilbene derivative combretastatin A-4 (CA-4, **1**, Fig. 1) [17,18]. Moreover, several studies have documented that compounds targeting the colchicine site also act as powerful vascular disrupting agents [19],

∗ Corresponding authors.
E-mail addresses: rmr@unife.it (R. Romagnoli), giampietro.viola.1@unipd.it (G. Viola).
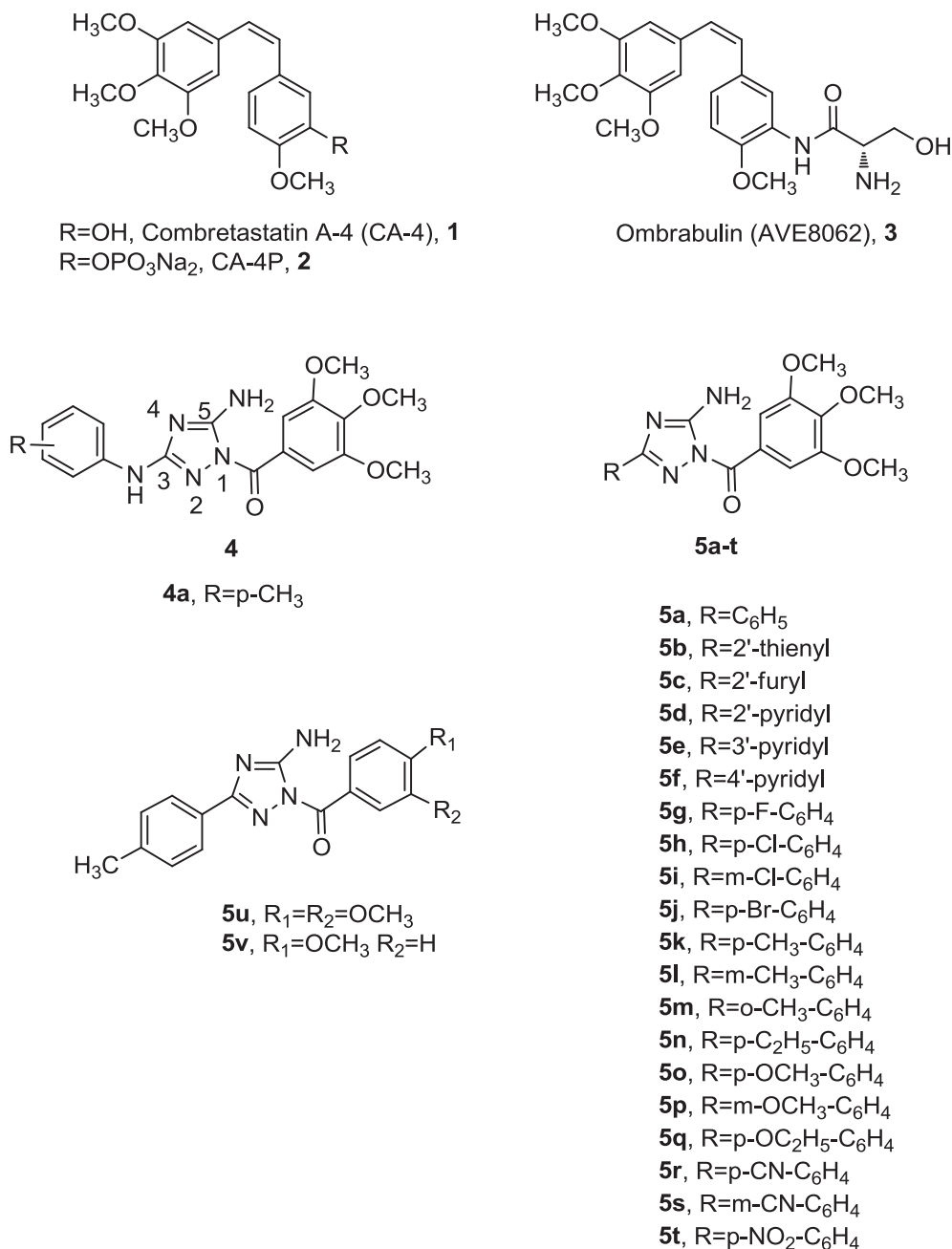
Fig. 1. Structures of CA-4 (**1**), CA-4P (**2**) and Ombrabulin (**3**). General structure of 1-(3′,4′,5′)-3-anilino-5-amino-1,2,4-triazole **4**. Molecular formulas of synthesized 1-aroyl-3-substituted-5-amino-1,2,4-triazoles **5a-v**.

particularly for the neovasculature of tumors.

While the vinca alkaloids and the taxoids have well-established roles in the treatment of human cancers, no colchicine site inhibitor is currently approved for cancer therapy, despite considerable synthetic efforts [20–22], including the preparation of many water-soluble prodrugs of CA-4, such as the phosphorylated derivative of combretastatin A-4 (CA-4P, **2**) in phase III clinical trials [23,24] or the serine amino acid prodrug of 3′-amino-deoxycombretastatin A-4 (Ombrabulin or AVE8062, **3**) [25], which is in phase I clinical studies for patients with solid tumors [26].

These observations emphasize the need to discover novel scaffolds active at the colchicine site and amenable to rapid derivatization because such compounds could be readily prepared in a cost-effective way by rapid and concise synthetic procedures [27]. In addition, several colchicine site binders have been shown to inhibit p53 mutant cell lines,

and this further emphasizes the importance of novel inhibitors of tubulin assembly that have activity against resistant tumors [28].

Among the synthetic inhibitors of tubulin polymerization, in a previous article we have reported the synthesis and biological evaluation of a series of compounds with general structure **4** based on the 1-(3′,4′,5′-trimethoxybenzoyl)-5-amino-1,2,4-triazole molecular skeleton, that showed strong antiproliferative activity against a panel of cell lines and act as inhibitors of microtubule polymerization by interfering with the colchicine site of tubulin [29]. Structure-activity relationships were elucidated with various substituents on the phenyl ring of the anilino moiety at the C-3 position of the 1,2,4-triazole ring, with the *p*-toluidino derivative **4a** exhibiting the best cell growth inhibitory activity among the tested compounds, with IC$_{50}$ values of 0.21–3.2 nM. This derivative was also a potent inhibitor of tubulin polymerization, with an IC$_{50}$ value of 0.75 μM for tubulin assembly.

2

A molecular docking study of compound **4a** in the colchicine site of tubulin showed that the trimethoxyphenyl unit of this derivative is placed in proximity of βCys241, while the phenyl ring of the aniline moiety at the 3-position of 1,2,4-triazole ring occupies a relatively small hydrophobic region deep in the binding site, establishing a series of non-polar interactions with amino acids βMet259, βThr314 and βLys352 in this subpocket, which stabilizes the binding of the molecule in the colchicine site. The same docking simulation on compound **4a** did not show any hydrogen bond interactions of the amino bridge function of the aniline moiety with the amino acid residues located in this small pocket of the colchicine site. X-ray crystallographic analysis on compound **4a** showed the formation of an intramolecular hydrogen bond between the carbonyl oxygen of the 3′,4′,5′-trimethoxybenzoyl function and the hydrogen of the amino moiety at the 1- and 5-position, respectively, of the 1,2,4-triazole ring.

Inspired by these observations and encouraged by the activity obtained with compound **4a**, here we report a new series of 1-(3′,4′,5′-trimethoxybenzoyl)-3-aryl/heteroaryl-5-amino-1,2,4-triazole analogues with general structure **5**, obtained by removing the amino function spacer of the anilino group of compounds with general structure **4**, connecting the aryl/heteroaryl moiety at the 3-position of 1,2,4-triazole ring and keeping constant the 3′,4′,5′-trimethoxybenzoyl function and the amino group at the 1- and 5-positions, respectively, of the triazole nucleus.

Thus, once the 1-(3′,4′,5′-trimethoxybenzoyl)-5-amino-1,2,4-triazole motif was identified as the minimum structural requirement for activity, modifications were focused on varying the substituent at the 3-position of the 1,2,4-triazole ring to develop new potent antiproliferative agents and to understand the minimum structural requirements for this class of compounds to exhibit potent and selective activity against cancer cell lines. The substituents examined included heterocycles such as thien-2-yl (**5b**), furan-2-yl (**5c**) and the three isomeric pyridines (**5d-f**) as well as the phenyl ring with various electron-withdrawing (F, Cl, Br, CN and NO_2) and electron-releasing (Me, Et, MeO and EtO) groups [30].

While for compounds **5a-t**, the 3′,4′,5′-trimethoxyphenyl of the benzoyl moiety at the *N*-1 position of the 1,2,4-triazole ring was kept unchanged because this ring is the essential structural requirement to maximize potency in a large series of inhibitors of tubulin polymerization, such as colchicine, steganacin, CA-4 and podophyllotoxin [31,32], in an effort to further confirm whether the 3,4,5-trimethoxybenzoyl moiety of compound **5k** played an essential role for antiproliferative activity, the corresponding 3,4-dimethoxybenzoyl and 4-methoxybenzoyl derivatives **5u** and **5v**, respectively, were prepared.

2. Chemistry

Synthesis of 1-aroyl-3-aryl/heteroaryl-5-amino-1,2,4-triazoles **5a-v** was accomplished using a three-step procedure described in Scheme 1.

The required 3-aryl/heteroaryl-5-amino-1,2,4-triazoles **8a-t** were synthesized by reaction of aroyl/heteroaroyl chloride **6a-t** with aminoguanidine hydrogen carbonate using pyridine as solvent to furnish the corresponding aroyl/heteroaryl amidoguanidines **7a-t**, followed by subsequent ring closure of the intermediate in water under microwave irradiation. Treatment of **8a-t** with an equimolar quantity of 3′,4′,5′-trimethoxybenzoyl chloride resulted in the formation of compounds **5a-t**. Using the same synthetic methodology, compounds **5u** and **5v** were prepared by the reaction of 3-(p-tolyl)-5-amino-1,2,4-triazole **8 k** with 4′,5′-dimethoxybenzoyl chloride and 4′-methoxybenzoyl chloride, respectively.

3. Biological results and discussion

3.1. In vitro antiproliferative activities.

The synthesized compounds **5a-v** were tested for their antiproliferative activity against a panel of five human cancer cell lines, *T*-leukemia (Jurkat), acute lymphoblastic leukemia (RS4;11), cervix carcinoma (HeLa), colon adenocarcinoma (HT29) and breast adenocarcinoma (MCF-7), by the MTT assay for 48 h. The results are summarized in Table 1, using CA-4 (**1**) and **4a** as positive controls. In general, the antiproliferative activities of compounds **5a**, **5h**, **5k-r** and **5u** were greater against the leukemia cells as compared with the solid tumor cells.
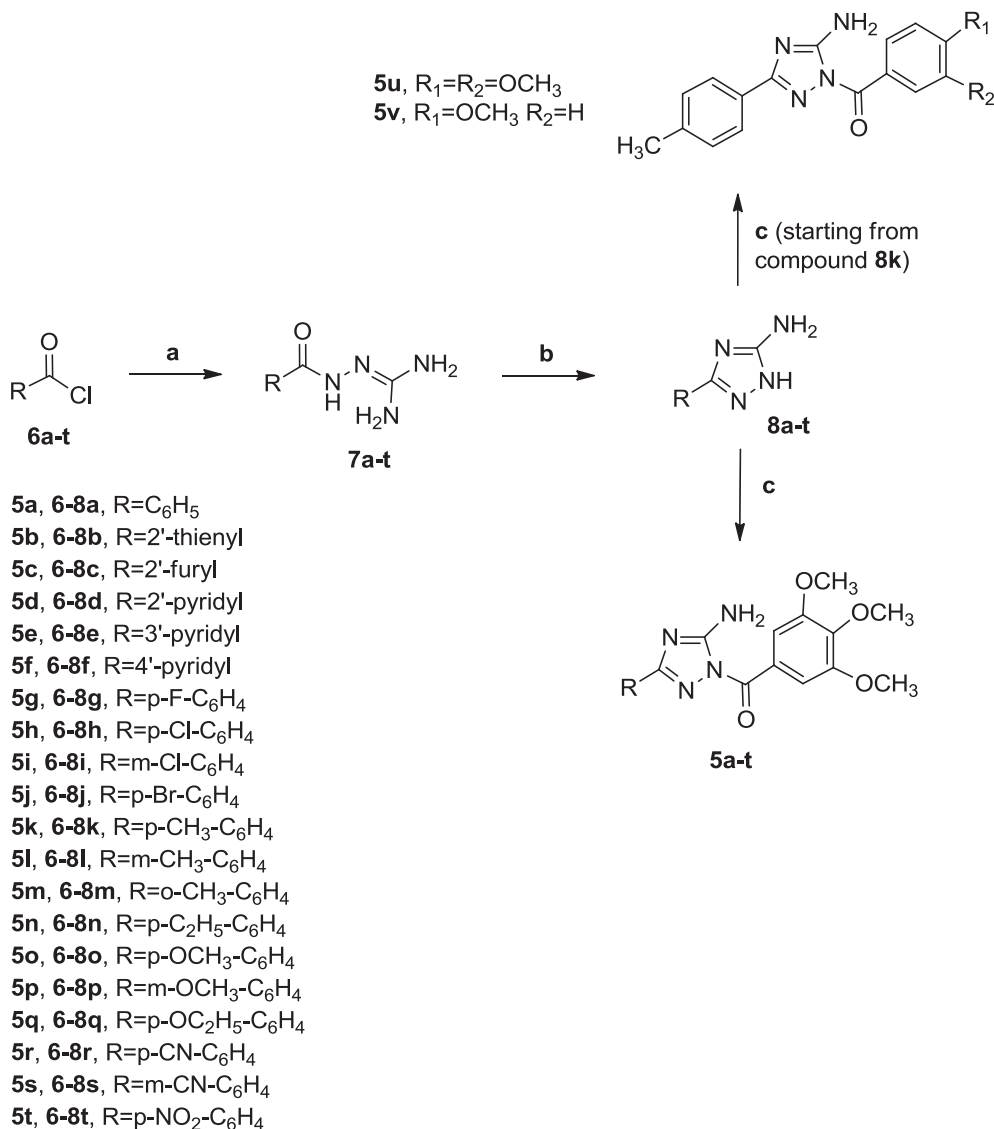
The unsubstituted phenyl derivative **5a** showed modest antiproliferative activity ($IC_{50} > 10 \mu M$) against HT29 and MCF-7 cells, while it was more active, with IC_{50} values of 1.4, 1.7 and 6.6 μM, against Jurkat, RS4;11 and HeLa cells, respectively.

In contrast, if the phenyl at position 3 was replaced by the biososteric 2′-thienyl (**5b**), 2′-furanyl (**5c**) or the three isomeric pyridines (compounds **5d-f**), significantly reduced activity was observed against the leukemia cell lines, while derivatives **5b-d**, but not **5e-f**, were comparable to **5a** against the solid tumor cells. Comparing the activities of *p*-tolyl and *p*-toluidino derivatives **5k** and **4a**, respectively, the presence of the amino (NH) spacer between the *p*-tolyl group and the 3-position of 1,2,4-triazole ring played a crucial role in affecting antiproliferative activity, with the *p*-tolyl derivative **5k** almost three orders of magnitude less potent than the *p*-toluidino derivative **4a**.

The data presented in Table 1 for compounds **5g-t** examine the effects of different substituents on the phenyl ring on antiproliferative activity. Considering the average IC_{50} against the five cell lines, compounds **5h**, **5j** and **5k** were the most active in the series, with mean IC_{50}'s, respectively, of 2.6, 2.5 and 3.3 μM. In addition, these data showed that the nature and the location of the substituent on the phenyl at the 3-position of the 1,2,4-triazole core played a critical role in antiproliferative activities, and only a few compounds showed any IC_{50} values lower than 1 μM against any of the cancer cell lines. RS4;11 and HT29 cells were the most sensitive to the *p*-bromophenyl derivative **5j**, with IC_{50} values of 0.8 and 0.5 μM, respectively. The *p*-tolyl compound **5k** showed an IC_{50} of 0.5 μM against the Jurkat cells, and the *p*-methoxyphenyl derivative **5o** and its isomeric *m*-methoxy analogue **5p** had IC_{50} values of 0.3 and 0.9 μM, respectively, against RS4;11 cells.

Substituents clearly had effects on antiproliferative activity. For example, antiproliferative activity was almost eliminated with a *m*-Cl (**5i**) or a *m*-CN (**5s**). Compounds with other *meta*-substituents, such as methyl (**5l**) or methoxy (**5p**), had reasonable activity relative to **5a** (in terms of mean IC_{50}, 8.6, 7.2 and 11.2 μM, respectively). With *para*-substituents, the best activities, in terms of mean IC_{50} values (2.5–3.3 μM) occurred with a *p*-Cl (**5h**), a *p*-Br (**5j**) and a *p*-CH_3 (**5k**). A second group of *para*-substituents had mean IC_{50} values in the 5.9–12.5 μM range (*p*-F, **5g**; *p*-ethyl, **5n**; *p*-methoxy, **5o**; *p*-ethoxy, **5q**; *p*-CN, **5r**). Compound **5t**, *p*-NO_2, was an outlier with a mean IC_{50} of 70.8 μM. With this large group of *para*-substituents, there was no clear pattern in terms of electron-withdrawing or electron-donating properties. The only compound with an *ortho*-substituent (**5m**, *o*-CH_3) was relatively inactive with a mean IC_{50} of 24 μM, as compared with 3.3 and 8.6 μM for its *para* and *meta* analogs **5k** and **5l**, respectively. In terms of position, *para* seems best, *ortho* worst, based on the methyl series **5k-m**. The superiority of the *para*-substituent over the *meta* held in every case except for the methoxy pair, where the mean IC_{50} for **5p** (*meta*) was 7.2 while that for **5o** (*para*) was 8.2.

Turning to individual cell lines, comparing the antiproliferative activities of compounds **5g** (*p*-F), **5h** (*p*-Cl) and **5j** (*p*-Br), revealed that on RS4;11, HeLa and HT-29 cells, the antiproliferative activity increased with increasing size of the halogen atom at the *para*-position of the phenyl ring. In contrast, for Jurkat and MCF7 cells, the effect of the halogen atom on activity was chlorine > bromine > fluorine. Thus, replacement of the fluorine at the *para*-position of the phenyl ring with a chlorine (compounds **5g** and **5h**, respectively) led to 6-, 3- and 2.5-fold increase of potency against Jurkat, RS4;11 and MCF-7 cells, while the activity was unchanged against HeLa and HT29 cells. Moving the chlorine from the *para*- to the *meta*-position on the phenyl ring

5u, R₁=R₂=OCH₃
5v, R₁=OCH₃ R₂=H

c (starting from compound **8k**)

6a-t → **a** → **7a-t** → **b** → **8a-t**

c

5a-t

5a, **6-8a**, R=C₆H₅
5b, **6-8b**, R=2'-thienyl
5c, **6-8c**, R=2'-furyl
5d, **6-8d**, R=2'-pyridyl
5e, **6-8e**, R=3'-pyridyl
5f, **6-8f**, R=4'-pyridyl
5g, **6-8g**, R=p-F-C₆H₄
5h, **6-8h**, R=p-Cl-C₆H₄
5i, **6-8i**, R=m-Cl-C₆H₄
5j, **6-8j**, R=p-Br-C₆H₄
5k, **6-8k**, R=p-CH₃-C₆H₄
5l, **6-8l**, R=m-CH₃-C₆H₄
5m, **6-8m**, R=o-CH₃-C₆H₄
5n, **6-8n**, R=p-C₂H₅-C₆H₄
5o, **6-8o**, R=p-OCH₃-C₆H₄
5p, **6-8p**, R=m-OCH₃-C₆H₄
5q, **6-8q**, R=p-OC₂H₅-C₆H₄
5r, **6-8r**, R=p-CN-C₆H₄
5s, **6-8s**, R=m-CN-C₆H₄
5t, **6-8t**, R=p-NO₂-C₆H₄

Scheme 1. Reagents. a: aminoguanidine hydrogen carbonate pyridine, 0 °C for 30 min. then 12 h rt; **b**: water, microwave irradiation, 100 W; **c**: 3′,4′,5′-(OMe)₃C₆H₂COCl for the preparation of **5a-t**, 4′,5′-(OMe)₂C₆H₃COCl or 4′-OMe-C₆H₄COCl for the synthesis of **5u** and **5v**, respectively, pyridine, 0 °C.

(compounds **5h** and **5i**, respectively) eliminated antiproliferative activity. A similar loss of potency was observed for the *para*-cyano derivative **5r** versus the isomeric *meta*-cyano analogue **5s**. Replacing *para*-chlorine with bromine (compounds **5h** and **5j**, respectively) had a contrasting effect. Derivative **5j** was 2-fold less potent than chlorine agent **5h** against Jurkat and MCF-7 cells, while it retained activity against HeLa cells. Nevertheless, the *p*-bromophenyl derivative **5j** showed strong antiproliferative activities in the submicromolar range against RS4;11 and HT29 cells, with IC₅₀ values of 0.8 and 0.5 μM, respectively, and was thus 2- and 7-fold more potent than its chlorine counterpart **5h**.

It should be noted that replacement of the weak electron-withdrawing fluorine with the weak electron-releasing methyl group, to furnish derivative **5k**, significantly improved potency from 2- to 16-fold against Jurkat, RS4;11 and MCF-7 cells, while the two derivatives showed similar activity toward HeLa and HT29 cells. However, the introduction of the methyl at the *para*-position of the phenyl ring (compound **5k**) enhanced activity from 3- to 5-fold against Jurkat, HT-29 and MCF-7 cells in comparison with the unsubstituted phenyl analogue **5a**, while the two compounds are equipotent against RS4;11 and HeLa cells.

To compare the effects of *ortho*-, *meta*- and *para*-methyl substitution on the phenyl ring, the *m*-tolyl and *o*-tolyl derivatives **5l** and **5m**, respectively, were also synthesized and showed different activities, indicating that the position of the methyl group is crucial for antiproliferative activity. The *o*-tolyl derivative **5m** was 3–70-fold less potent the *p*-tolyl analogue **5k**, whereas the *m*-tolyl derivative **5l** had intermediate activity, being 2–7-fold less active than the *p*-tolyl isomer **5k** against all cancer cell lines.

As noted above, our findings indicate that a methoxy group located at the *para*-position of the phenyl ring (compound **5o**) resulted in strong antiproliferative activity against RS4;11 cells (IC₅₀ = 0.3 μM), while shifting it to the *meta*-position, to furnish derivative **5p**, decreased activity 3-fold. A similar effect was observed against Jurkat and HeLa cells. Additionally, our findings indicate that moving substituents from the *para*- to the *meta*- or *ortho*-position on the phenyl ring was generally not favorable for maintaining antiproliferative activity within the series of analogues reported here (**5h** *vs.* **5i**, **5k** *vs.* **5l** and **5m**, **5o** *vs.* **5p** and **5r** *vs.* **5s**).

Replacement of *p*-methoxy with *p*-ethoxy (compounds **5o** and **5q**, respectively) reduced activity from 2- to 28-fold against Jurkat, RS4;11, Hela and MCF-7 cells, although activity was retained against HT29 cells.

Compound **5u**, with a 3′,4′-dimethoxybenzoyl group at the N₁-

4

Table 1
In vitro inhibitory effects of compounds **4a**, **5a-v** and **CA-4**.

Compd	IC_{50}[a] (µM)					
	Jurkat	RS4;11	HeLa	HT29	MCF-7	Average
5a	1.4 ± 0.3	1.7 ± 0.1	6.6 ± 1.3	27.3 ± 9.6	19.1 ± 2.0	11.2
5b	43.3 ± 7.3	17.7 ± 7.7	10.5 ± 2.1	15.9 ± 1.3	19.9 ± 3.1	21.5
5c	> 100	44.3 ± 16.8	21.3 ± 1.6	18.5 ± 2.2	19.1 ± 1.1	nc
5d	> 100	10.8 ± 3.2	17.7 ± 1.3	23.9 ± 2.6	21.9 ± 3.1	nc
5e	> 100	68.3 ± 10.9	> 100	> 100	> 100	nc
5f	> 100	49.0 ± 4.6	> 100	> 100	> 100	nc
5g	8.1 ± 1.3	4.0 ± 0.5	5.4 ± 1.6	4.7 ± 1.5	7.2 ± 3.2	5.9
5h	1.4 ± 0.8	1.3 ± 0.5	4.0 ± 0.5	3.8 ± 1.4	2.7 ± 0.7	2.6
5i	> 100	> 100	> 100	> 100	> 100	> 100
5j	2.6 ± 0.6	0.8 ± 0.2	2.8 ± 0.9	0.5 ± 0.1	5.6 ± 1.6	2.5
5k	0.5 ± 0.2	1.8 ± 0.06	5.5 ± 1.4	4.9 ± 0.8	3.6 ± 1.0	3.3
5l	3.9 ± 0.1	4.2 ± 0.9	10.1 ± 2.6	13.2 ± 1.8	11.5 ± 1.4	8.6
5m	34.0 ± 0.6	19.3 ± 0.9	19.8 ± 3.1	25.2 ± 2.5	23.6 ± 3.6	24.4
5n	2.6 ± 0.09	2.2 ± 0.1	15.6 ± 1.9	21.1 ± 2.9	18.6 ± 2.1	12.0
5o	1.2 ± 0.5	0.3 ± 0.1	6.6 ± 1.3	23.4 ± 2.1	9.6 ± 1.5	8.2
5p	4.0 ± 1.3	0.9 ± 0.02	9.8 ± 1.2	11.2 ± 1.1	10.3 ± 2.0	7.2
5q	4.3 ± 0.8	8.5 ± 1.5	11.2 ± 2.3	19.9 ± 1.6	18.8 ± 2.6	12.5
5r	4.0 ± 0.1	3.6 ± 1.1	9.8 ± 1.1	12.1 ± 1.5	10.2 ± 0.9	7.9
5s	> 100	99.3 ± 22.8	> 100	> 100	> 100	nc
5t	59.3 ± 17.6	47.7 ± 9.3	75.6 ± 3.5	88.9 ± 5.2	82.3 ± 3.9	70.8
5u	9.3 ± 1.1	1.8 ± 0.6	15.1 ± 1.9	17.2 ± 2.5	13.2 ± 1.6	11.3
5v	> 100	38.9 ± 7.2	45.5 ± 3.6	65.3 ± 4.2	39.3 ± 4.1	nc
4a (nM)	0.8 ± 0.3	nd	3.2 ± 1.3	0.8 ± 0.1	1 ± 0.6	nc
CA-4 (nM)	0.8 ± 0.2	370 ± 100	4 ± 1	180 ± 30	5 ± 0.6	112

nc = not calculated.

nd = not determined.

[a] IC_{50} = compound concentration required to inhibit tumor cell proliferation by 50%.

position of the 3-(*p*-toly)-5-amino-1,2,4-triazole system, had 3–18-fold reduced cell growth inhibitory activity as compared with the 3′,4′,5′-trimethoxybenzoyl derivative **5k** against four of the five cell lines, but the two derivatives were equipotent against RS4;11 cells. The 4′-methoxybenzoyl analogue **5v** showed substantially reduced activity (IC_{50} > 30 µM) compared to **5k** in all cell lines.

Among the electron-withdrawing groups, introduction of the nitro substituent, resulted in compound (**5t**) with reduced antiproliferative activity compared with those bearing halogen or cyano substituents.

In summary, small structural modifications are responsible for great variations of the IC_{50} values obtained against the cancer cell lines studied, with the methyl and methoxy moieties (compounds **5k** and **5o**, respectively) being optimal at the *para*-position of the phenyl at the 3-position of the 1,2,4-triazole ring.

3.2. In vitro inhibition of tubulin polymerization and colchicine binding.

To investigate whether the antiproliferative activities of selected substituted phenyl derivatives **5j** (*p*-Br), **5k** (*p*-Me), **5o** (*p*-OMe) and **5p** (*m*-OMe) derived from an interaction with tubulin, these agents were evaluated for their ability to inhibit tubulin polymerization and for effects on the binding of [³H]colchicine to tubulin (Table 2). For comparison, CA-4 (**1**) and **4a** were examined in contemporaneous experiments as reference compounds.

The *p*-tolyl derivative **5k**, the most potent compound of the series against Jurkat (*T*-leukemia) cells, was found to be also a strong inhibitor of tubulin polymerization, with an IC_{50} value of 0.66 µM, nearly twice as potent as CA-4 (IC_{50}:1.2 µM). Note that **4a** had much greater antiproliferative activity than **5k**, despite the similar effects on tubulin assembly. Such discrepancies in antitubulin versus antiproliferative activity are not infrequently observed, but the reasons are usually uncertain, as is the case here. Among possible explanations is that we are using bovine brain tubulin in the former studies, and its composition in terms of tubulin isotypes differs significantly from that of different human cancer cell lines [33].

Compound **5o**, as the most potent derivative of the series against

Table 2
Inhibition of tubulin polymerization and colchicine binding by compounds **CA-4**, **4a**, **5j-k** and **5o-p**.

Compound	Tubulin assembly[a] IC_{50} ± SD (µM)	Colchicine binding [b] % ± SD
5j	> 20	17 ± 6
5k	0.66 ± 0.09	61 ± 4
5o	0.97 ± 0.1	51 ± 3
5p	> 20	3.8 ± 0.2
4a	0.75 ± 0.1	92 ± 2
CA-4	1.2 ± 0.1	98 ± 0.5

[a] Inhibition of tubulin polymerization. Tubulin was at 10 µM.

[b] Inhibition of [³H]colchicine binding. Tubulin, colchicine and tested compound were at 1, 5 and 5 µM, respectively.

RS4;11 (acute lymphoblastic leukemia) cells, strongly inhibited tubulin polymerization (IC_{50}:0.97 µM) with activity comparable to that of CA-4. The results obtained demonstrate that the antiproliferative activities of compounds **5k** and **5o** are related to inhibition of tubulin polymerization. It is intriguing to note that compounds **5j** and **5p** were inactive as inhibitors of tubulin polymerization, with minimal activity (IC_{50} > 20 µM), although these derivatives demonstrated significant antiproliferative activity against RS4;11 cells, with IC_{50} values of 0.8 and 0.9 µM, respectively, only 3-fold less potent as antiproliferative agents relative to **5o** against this cancer cell line. The weak activity against tubulin suggests the possibility that compounds **5j** and **5p** may possess an additional mechanism of inhibition of cancer cell growth beyond that attributable to the tubulin-based mechanism.

Comparing the IC_{50} values of the inhibition of tubulin assembly for compounds **5o** and **5p**, corresponding to 0.97 and > 20 µM, respectively, it appears that a small structural modification, such as moving the methoxy group from the *para*- to the *meta*-position of the phenyl ring, is responsible for great variation in antitubulin activity, suggesting that there is a space-limited pocket surrounding the phenyl at the 3-position of 1,2,4-triazole ring.

In the colchicine binding studies, compounds **5k** and **5o** displayed

61% and 51%, respectively, inhibition of [3H]colchicine binding at 5 μM, with 1 μM tubulin. Both compounds were significantly less potent than CA-4 in this assay, despite their greater potency as inhibitors of tubulin assembly. Such differences are commonly observed, and CA-4 is a particularly potent inhibitor of [3H]colchicine binding [17,18]. The data suggested that compounds 5k and 5o bind to the colchicine site and inhibit the polymerization of tubulin. In this assay, derivative 4a potently inhibited the binding of [3H]colchicine to tubulin, and with 92% inhibition was 1.5-fold more active than 5k, which in this experiment inhibited colchicine binding by 61%.

In general, in these experiments, inhibition of [3H]colchicine binding correlated more closely with inhibition of tubulin assembly than with antiproliferative activity. Thus, compound 5o was as active as CA-4 as an inhibitor of tubulin polymerization, although this derivative was less active in its effects on cell growth against the whole panel of cancer cell lines.

3.3. Molecular modeling studies

In order to further understand the different activity profiles of the tested compounds, several molecular modeling studies were performed. According to a recent publication, the tubulin colchicine domain is formed by a main site, where colchicine binds (zone 1), and two additional neighboring pockets (zones 2 and 3) [34]. After studying the tubulin crystal structures in complex with different ligands, these authors concluded that globular or butterfly like shaped molecules bind to zones 1 and 2, mimicking colchicine binding, whereas planar compounds tend to bind in zones 2 and 3 [34]. In order to identify the most likely binding area of the new derivatives, a series of docking studies were performed with compounds 5j, 5k, 5o and 5p. Two different tubulin crystal structures were used: one co-crystallized with colchicine (PDB ID: 4O2B), representing the colchicine-like binding site area (zones 1 and 2), and one co-crystallized with the inhibitor G2N (PDB ID: 3N2G), representing the planar compounds binding in zones 2 and 3 [35,36]. The 3N2G crystal structure was chosen because the ligand included a free amino group in the central portion of G2N, which is a feature also present in the compounds we examined. Docking studies were performed using the Glide SP method, and the results were then refined using Glide XP scoring [37]. The proposed binding modes of the two active derivatives 5k and 5o in the colchicine binding site are consistent with that previously reported for similar derivatives, and these binding modes are very similar to that found for the co-crystallized colchicine. In these models, the trimethoxyphenyl ring is in proximity of βCys241, with the 4′-methylphenyl or the 4′-methoxyphenyl ring occupying the area close to βMet259 [29] (Fig. 2A).

We found no plausible binding poses for the two inactive compounds, 5p and 5j, by the docking program, but there was a binding pose for 5p (shown in Fig. 2B), where the 3-methoxyphenyl ring pointed in the opposite direction relative to the co-crystallized colchicine. We then examined the potential binding mode of the new compounds into the G2N site. Even though the compounds occupy the binding site in a very similar manner to the co-crystallized inhibitor, it was not possible to rationalize the differences seen in the tubulin polymerization inhibition assay, which appeared to be linked to the substituent on the phenyl ring (Fig. 3A and B).

Based on the docking results, a binding mode similar to that of colchicine might be more relevant for these compounds (zone 1). However, the planar conformation of the molecules and the relatively low colchicine binding competition values found in the biological assay, would suggest that the binding site for these new compounds only partially overlaps the one for colchicine and could involve only zones 2 and 3 (3N2G).

Therefore, in order to help select the potential binding site from the two choices presented in Figs. 2 and 3, a series of short 20 ns molecular dynamic (MD) simulations on selected compounds (5k, 5o, 5p) were performed using the Desmond software package [38]. The relative
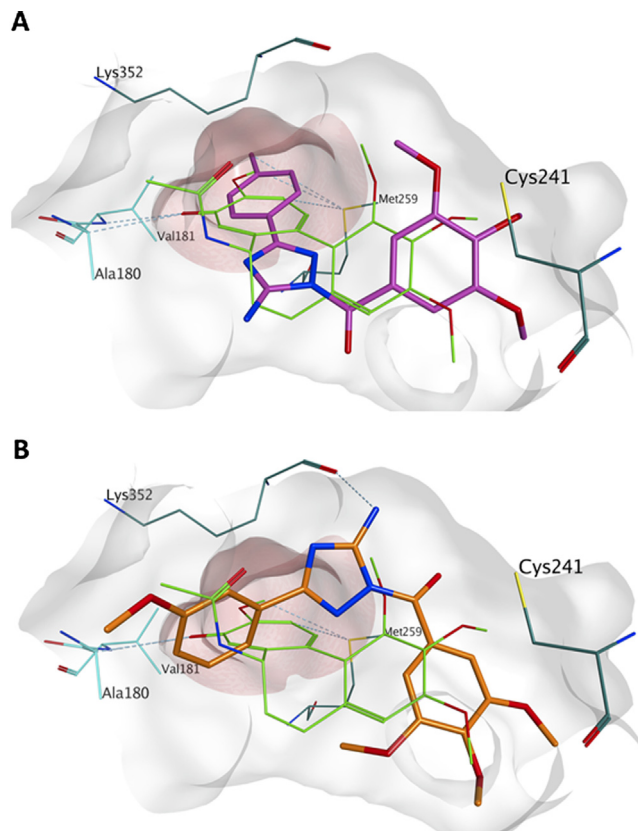

Fig. 2. Proposed binding for compound 5k (A, carbon atoms in purple) and 5p (B, carbon atoms in orange) in the colchicine binding site (4O2B). Co-crystallized colchicine is shown in green. The hydrophobic subpocket nearby, including βMet259, is highlighted with a red surface. Note how the 3′-methoxyphenyl ring of 5p is pointing in the opposite direction of the co-crystallised colchicine, as compared with the analogous structural feature of 5k as shown in Panel A. (For interpretation of the references to colour in this figure legend, the reader is referred to the web version of this article.)

binding free energies (ΔG$_{binding}$) of the compounds were then calculated using the Prime/MM-GBSA based calculation method [39]. All the protein-ligand systems reached stability after an initial 6 ns of equilibration, as shown by the C-alpha RMSD variation (see Fig. S1 in the Supporting Information data), so therefore only the remaining 14 ns of the simulation were considered in our analysis.

The position of the trimethoxyphenyl ring and the disposition of the substituted phenyl ring near the area of βMet259 were maintained during the entire simulation of 5k and 5o, confirming the reliability of the docking in predicting the binding mode in the colchicine binding site (4O2B). In particular, water bridge formation between the methoxy groups and βCys241 and the interaction between βLys352 and the central triazole ring were seen for both derivatives during the entire MD, potentially contributing to protein-ligand stability (Fig. 4A). Instead, the proposed binding for 5p was very variable, with the compound not able to occupy in a stable manner the binding area during the whole simulation. In the case of the G2N binding site, for all the derivatives studied, the trimethoxyphenyl ring was no longer able to interact with βCys241, moving away from this residue and potentially losing a fundamental interaction point for the tubulin inhibition function (Fig. 4B). Table 3 reports the calculated ligand-interaction energies with the two different binding sites for the compounds analysed by MD. Overall, the ΔG$_{binding}$ calculated for 5k and 5o in the colchicine binding site (4O2B) is lower than the one estimated for each corresponding compound in the G2N binding area, potentially meaning that the colchicine binding site ligands system is more stable in comparison with the G2N-binding site ligands system, and therefore the former is the
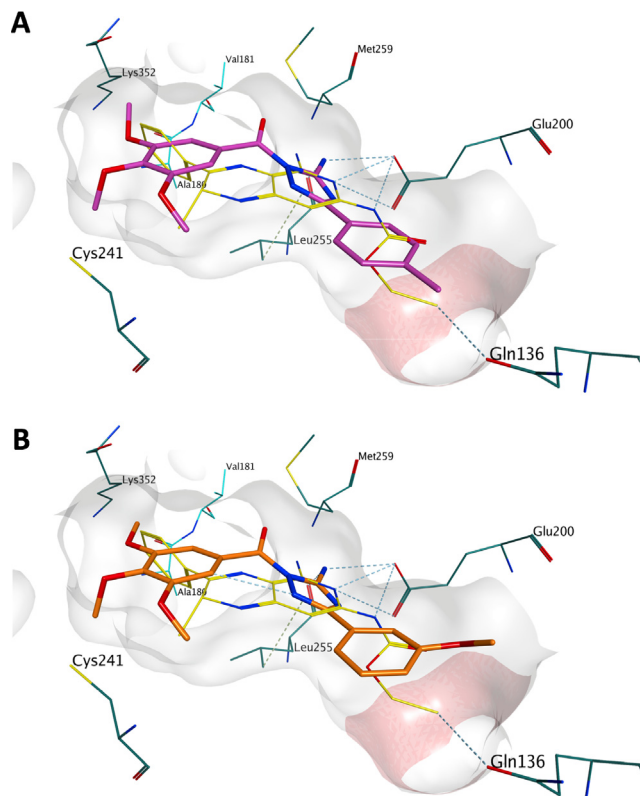
Fig. 3. Proposed binding for compound **5k** (A, carbon atoms in purple) and **5p** (B, carbon atoms in orange) in the G2N binding site (3N2G). Co-crystallized G2N is shown in yellow. The different location of this binding site in comparison with the colchicine binding site, can be easily seen by noting the spatial orientation of βCys241. No substantial differences in the binding modes were found between the active (**5k**) and inactive (**5p**) derivatives. (For interpretation of the references to colour in this figure legend, the reader is referred to the web version of this article.)

more likely binding area for the these new derivatives.

Water bridge formation between the methoxy groups and βCys241, the interaction between βLys352 and the central 1,2,4-triazole ring and the accommodation of the substituted phenyl ring in the hydrophobic sub-pocket near βMet259 could confer stability on the protein-ligand system leading to lower energy values, reflecting binding of the ligand resulting in inhibition of tubulin polymerization. The insertion of the methoxy group in position 3′, as in compound **5p**, abolishes inhibition

Table 3
Calculated ligand-interaction energies for the compounds analyzed by MD simulation.

Compound	$\Delta G_{binding}$ (kJ/mol)[a] ± SD 4O2B	$\Delta G_{binding}$ (kJ/mol)[a] ± SD 3N2G
5k	−69.512 ± 1.769	−58.685 ± 3.338
5o	−74.471 ± 0.400	−69.161 ± 3.379
5p	−59.613 ± 1.964	−65.809 ± 2.318

[a] Average values calculated as mean of three $\Delta G_{binding}$ obtained from three independent MD simulations (triplicate) for each compound. For each replicate, the average $\Delta G_{binding}$ value was calculated excluding the first 6 ns of MD in which the protein-ligand system reached stability. Standard deviation (SD) is reported.

of tubulin polymerization, and a completely different binding pose with a higher calculated $\Delta G_{binding}$ value was found. The higher $\Delta G_{binding}$ values obtained for the G2N-binding site is an indication that the protein-ligand system could be less stable if the compounds bind to this site. Moreover, the higher standard deviation calculated for the three average $\Delta G_{binding}$ values may indicate that the ligand binding in this area was very variable in all the performed simulations, giving a further indication that it is very unlikely that the G2N-binding site is the potential binding site for these new derivatives.

3.4. Analysis of cell cycle effects

The effects of 24 h treatments with different concentrations of **5k** and **5p** on cell cycle progression in HeLa cells were determined by flow cytometry (Fig. 5). Compound **5k** caused a significant G2/M arrest in a concentration-dependent manner in HeLa cells, with an increase in G2/M cells occurring at 5 μM. The cell cycle arrest in G2/M phase was accompanied by a slight reduction of both G1 and S phase cells. In contrast, treatment with compound **5p** even at high concentrations (20 μM) had no effect on cell cycle distribution, and, in particular, it did not cause the increase in G2-M cells always observed with antitubulin agents, in good agreement with the negative result observed in the tubulin polymerization assay. It is worthwhile noting that similar results wereb also obtained after 48 h treatments (data not shown).

3.5. Compounds **5k** and **5p** both induce apoptosis

To evaluate the mode of cell death induced by **5k** and **5p**, a biparametric cytofluorimetric analysis was performed using propidium iodide (PI), which stains DNA and enters only dead cells, and fluorescent immunolabeling of the protein annexin-V, which binds to phosphatidyl serine in a highly selective manner. Dual staining for
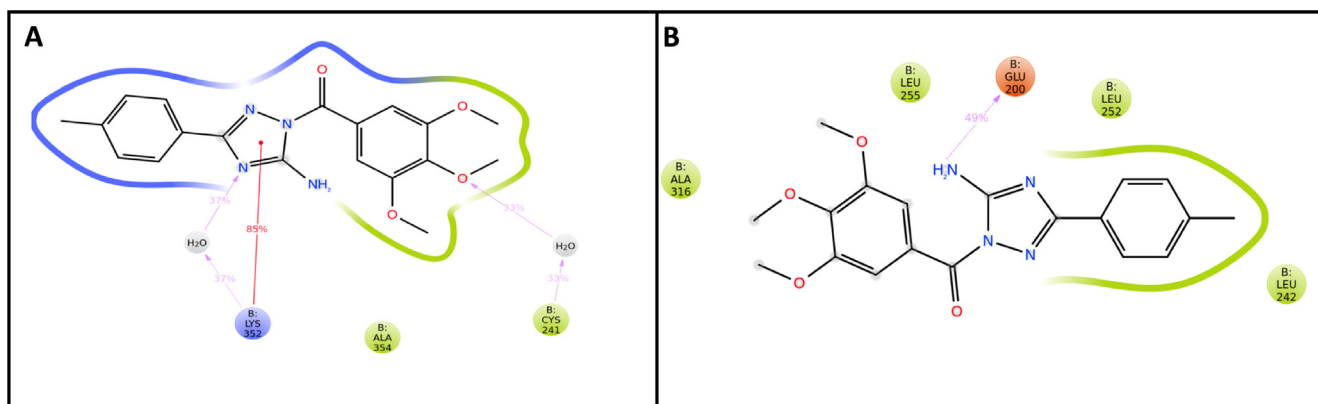

Fig. 4. Ligand-protein interaction diagram for compound **5k** in the two different binding sites, 4O2B (a) and 3N2G (b). The most persistent interactions formed during the MD simulation are reported together with the interaction strengths. The interaction between the methoxy groups and βCys241, mediated by a water bridge, is only present in the colchicine binding site simulation. The first 6 ns of MD, in which the protein-ligand system reached stability, were excluded from the diagram.
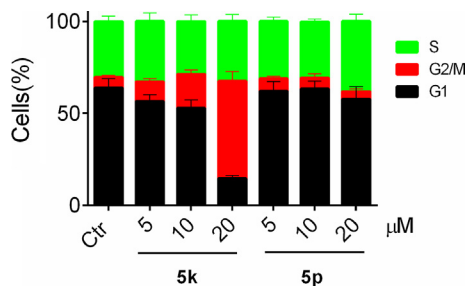
Fig. 5. Percentage of cells in each phase of the cell cycle in HeLa cells treated with compounds **5k** and **5p** at the indicated concentrations for 24 h. Cells were fixed and labeled with PI and analyzed by flow cytometry as described in the Experimental Section. Data are expressed as mean ± SEM.

annexin-V and with PI permits discrimination between live cells (annexin-V$^-$/PI$^-$), early apoptotic cells (annexin-V$^+$/PI$^-$), late apoptotic cells (annexin-V$^+$/PI$^+$) and necrotic cells (annexin-V$^-$/PI$^+$). As shown in Fig. 6, HeLa cells treated with **5k** or **5p** showed an accumulation of annexin-V positive cells in comparison with the control, in a concentration- and time-dependent manner.

4. Conclusions

We have discovered a new class of simple synthetic inhibitors of tubulin polymerization based on the 1-(3′,4′,5′-trimethoxybenzoyl)-3-aryl/heteroaryl-5-amino-1,2,4-triazole molecular skeleton. The introduction of different electron-withdrawing (F, Cl and Br) and electron-releasing (Me and OMe) groups at the *para*-position of the phenyl ring had variable effects on cell growth inhibitory activity against different cancer cell lines, revealing an avenue for future optimization. An enhancement of antiproliferative activity was observed against leukemic RS4;11 cells by the introduction of a bromine or a methoxy group at the *para*-position of the phenyl ring or moving the methoxy group

from the *para*- to the *meta*-position (compounds **5j**, **5o** and **5p**, respectively).

Only compounds **5j** (*p*-Br), **5k** (*p*-Me), **5o** (*p*-OMe) and **5p** (*m*-OMe) showed cell growth inhibitory activities in the submicromolar range (IC$_{50}$ < 1 μM) against selected cancer cell lines, with **5j**, **5k** and **5o** as the most potent antiproliferative agents against HT29, Jurkat and RS4;11 cells, with IC$_{50}$ values of 0.5, 0.5 and 0.3 μM.

Compounds **5k** and **5o**, the most potent antiproliferative agents against Jurkat and RS4;11 leukemic cells, respectively, proved to be strong inhibitors of tubulin polymerization (IC$_{50}$:0.66 μM for **5k**, IC$_{50}$:0.97 μM for **5o**). These findings indicate that the *p*-tolyl as well as the *p*-methoxyphenyl at the 3-position of 5-amino-1,2,4-triazole core are crucial moieties for inhibition of tubulin polymerization. Analogues **5j** (*p*-Br) and **5p** (*m*-OMe), with antiproliferative activity at submicromolar concentrations against RS4;11 cells, showed IC$_{50}$ > 20 μM in the tubulin polymerization assay. This, together with the minimal cell cycle effect of **5p**, implies that these derivatives act against another target. The complete loss of antitubulin activity of the *m*-OMe analogue **5p** as compared with the *p*-OMe counterpart **5o** was presumably due primarily to steric limitations around the phenyl ring at the C-3 position of the 1,2,4-triazole core. Although derivatives **5j** and **5p** were 3-fold less active as antiproliferative agents as compared with compound **5o** against RS4;11 cells, the weak tubulin polymerization inhibition of **5j** and **5p** suggested that the mechanism of antiproliferative activity of these two molecules was different from inhibition of tubulin polymerization. These results were also confirmed by analysis of cell cycle data in which only compound **5k** arrested cells in the G2/M phase, in good agreement with the tubulin polymerization data. Removing the amino spacer between the *p*-tolyl moiety and the 1,2,4-triazole ring of **4a**, to furnish derivative **5k**, resulted in a substantial reduction in antiproliferative activity, while the two compounds were equipotent as inhibitors of tubulin polymerization. Assuming similar tubulin content in the different cell lines, the most reasonable explanation for these differences is that the tubulin assay is not a good predictor of antiproliferative activity in cells.
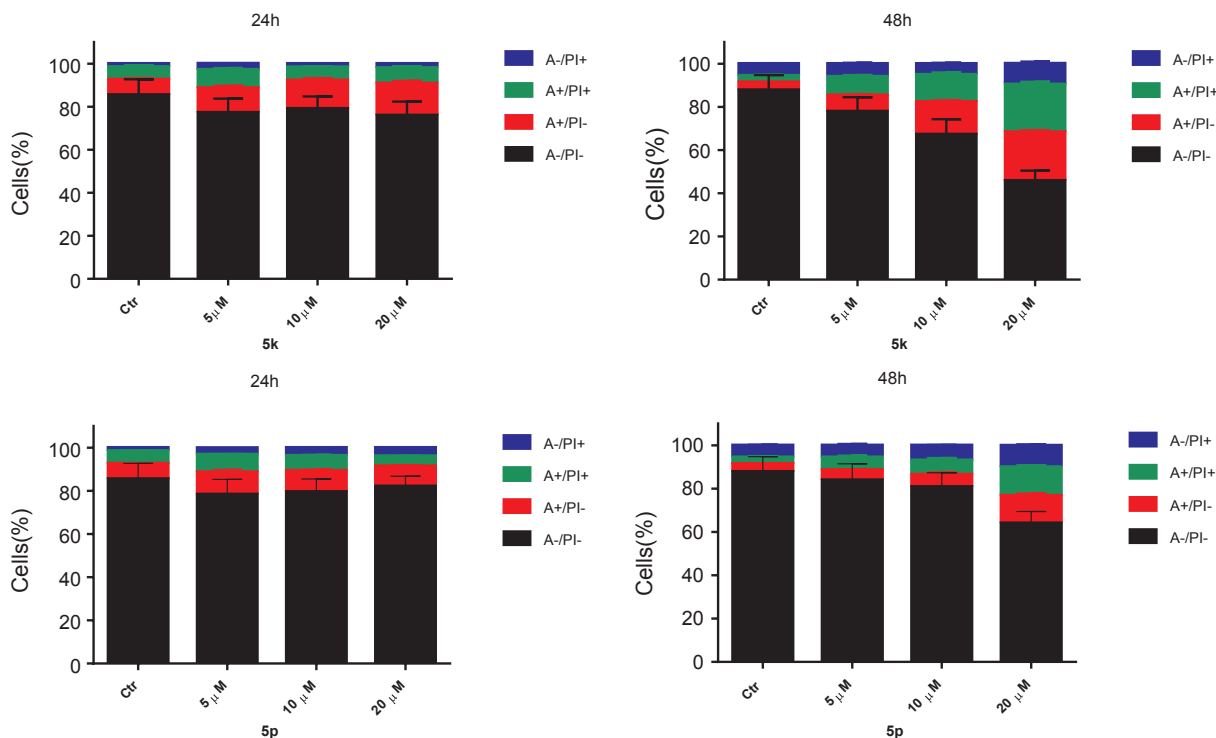

Fig. 6. Flow cytometric analysis of apoptotic cells after treatment of HeLa cells with compounds **5k** or **5p** at the indicated concentrations after incubation for 24 or 48 h. The cells were harvested and labeled with annexin-V-FITC and PI and analyzed by flow cytometry. Data are represented as mean ± SEM of three independent experiments.

Finally, several compounds, such as **5j**, **5k**, **5o** and **5p**, retain anti-proliferative activity at submicromolar levels toward leukemic cells, and this should permit the future design of compounds specifically directed against leukemia.

5. Experimental protocols

5.1. Chemistry

5.1.1. Materials and methods

^{1}H NMR spectra were recorded on either a Bruker AC 200 or a Varian 400 Mercury Plus spectrometer, while ^{13}C NMR spectra were recorded on Varian 400 Mercury Plus spectrometer. Chemical shifts (δ) are given in ppm upfield from tetramethylsilane as internal standard, and the spectra were recorded in appropriate deuterated solvents, as indicated. Positive-ion electrospray ionization (ESI) mass spectra were recorded on a double-focusing Finnigan MAT 95 instrument with BE geometry. Melting points (mp) were determined on a Buchi-Tottoli apparatus and are uncorrected. Microwave-assisted reactions were performed on a CEM Discover SP single-mode reactor (2450 MHz). Closed vessel experiments were carried out in capped microwave-dedicated vials (10 mL). The temperature of the reaction was monitored by an external fiber optic temperature sensor. After completion of the reaction, the mixture was cooled to 25 °C via air-jet cooling. All products reported showed ^{1}H and ^{13}C NMR spectra in agreement with the assigned structures. The purity of tested compounds was determined by combustion elemental analyses conducted by the Microanalytical Laboratory of the Chemistry Department of the University of Ferrara with a Yanagimoto MT-5 CHN recorder elemental analyzer. All tested compounds yielded data consistent with a purity of at least 95% as compared with the theoretical values. All reactions were carried out under an inert atmosphere of dry nitrogen. Standard syringe techniques were used for transferring dry solvents. Reaction courses and product mixtures were routinely monitored by TLC on silica gel (precoated F_{254} Merck plates), and compounds were visualized with aqueous $KMnO_4$. Flash chromatography was performed using 230–400 mesh silica gel and the indicated solvent system. Organic solutions were dried over anhydrous Na_2SO_4.

5.1.2. General method A for the synthesis of compounds 7a-t.

To a stirred solution of aminoguanidine hydrogen carbonate (2.8 g, 20 mmol) in dry pyridine (30 mL) cooled at 0 °C was added the appropriate hetero/aroyl chloride **6a-t** (20 mol, 1 equiv.) in small portions. The reaction mixture was stirred for 30 min at 0 °C and then overnight at room temperature. Pyridine was removed by evaporation under reduced pressure, and the residue was dissolved with water (20 mL). The stirred solution was cooled with an ice bath, and an aqueous solution of NaOH (2N) was slowly added (pH = 10–11). The resultant solid was collected by filtration, washed with ethyl ether (15 mL) and dried overnight under vacuum on P_2O_5 to afford compounds **7a-t**. Compounds **7a** and **7f** showed spectroscopic and analytical data in agreement with those previously published [40]. Compounds **7e**, **7f**, **7h**, **7i** and **7o** were previously published, although neither their spectroscopic and analytical data were reported [30].

5.1.2.1. 2-Benzoylhydrazinecarboximidamide (7a). Synthesized according to method **A**, compound **7a** was obtained as a white solid (yield 61%); mp 184–185 °C. ^{1}H NMR (d_6-DMSO) δ: 6.84 (bs, 2H), 6.98 (bs, 2H), 7.28 (m, 3H), 7.86 (m, 2H), 10.5 (bs, 1H). MS (ESI): $[M+1]^+ = 179.25$.

5.1.2.2. 2-(Thiophene-2-carbonyl)hydrazinecarboximidamide (7b). Synthesized according to method **A**, derivative **7b** was obtained as a yellow solid (yield 53%); mp 210–212 °C. ^{1}H NMR (d_6-DMSO) δ: 6.77 (bs, 4H), 6.94 (dd, J = 4.8 and 3.6 Hz, 1H), 7.33 (m, 2H), 10.4 (bs, 1H). MS (ESI): $[M+1]^+ = 185.07$.

5.1.2.3. 2-(Furan-2-carbonyl)hydrazinecarboximidamide (7c). Synthesized according to method **A**, derivative **7c** was obtained as a white solid (yield 44%); mp 214–215 °C. ^{1}H NMR (d_6-DMSO) δ: 6.39 (dd, J = 3.2 and 1.6 Hz, 1H), 6.57 (d, J = 3.2 Hz, 1H), 6.67 (bs, 4H), 7.51 (d, J = 1,6 Hz, 1H), 10.4 (bs, 1H). MS (ESI): $[M+1]^+ = 169.22$.

5.1.2.4. 2-Picolinoylhydrazinecarboximidamide (7d). Synthesized according to method **A**, derivative **7d** was obtained as a yellow solid (yield 54%); mp 210–211 °C. ^{1}H NMR (d_6-DMSO) δ: 6.78 (bs, 4H), 7.62 (dd, J = 6.8 and 7.0 Hz, 1H), 8.06 (m, 1H), 8.72 (d, J = 6.8 Hz, 1H), 9.10 (d, J = 2.0 Hz, 1H), 10.3 (bs, 1H). MS (ESI): $[M+1]^+ = 180.56$.

5.1.2.5. 2-Nicotinoylhydrazinecarboximidamide (7e). Synthesized according to method **A**, derivative **7e** was obtained as a yellow solid (yield 62%); mp 203–205 °C. ^{1}H NMR (d_6-DMSO) δ: 6.86 (bs, 4H), 7.26 (m, 1H), 8.19 (dd, J = 5.8 and 2.0 Hz, 1H), 8.43 (dd, J = 4.8 and 1.6 Hz Hz, 1H), 9.10 (d, J = 2.0 Hz, 1H), 10.2 (bs, 1H). MS (ESI): $[M+1]^+ = 180.24$.

5.1.2.6. 2-Isonicotinoylhydrazinecarboximidamide (7f). Synthesized according to method **A**, derivative **7f** was obtained as a yellow solid (yield 56%); mp 187–189 °C. ^{1}H NMR (d_6-DMSO) δ: 6.94 (bs, 4H), 7.82 (dd, J = 4.4 and 1.2 Hz, 2H), 8.47 (dd, J = 4.4 and 1.2 Hz, 2H), 10.2 (bs, 1H). MS (ESI): $[M+1]^+ = 180.36$.

5.1.2.7. 2-(4-Fluorobenzoyl)hydrazinecarboximidamide (7g). Synthesized according to method **A**, compound **7g** was obtained as a white solid (yield 50%); mp 187–188 °C. ^{1}H NMR (d_6-DMSO) δ: 6.74 (bs, 2H), 6.86 (bs, 2H), 7.02 (t, J = 9.0 Hz, 2H), 7.93 (dd, J = 9.0 and 6.2 Hz, 2H), 10.4 (bs, 1H). MS (ESI): $[M+1]^+ = 197.21$.

5.1.2.8. 2-(4-Chlorobenzoyl)hydrazinecarboximidamide (7h). Synthesized according to method **A**, compound **7h** was obtained as a yellow solid (yield 43%); mp 188–189 °C. ^{1}H NMR (d_6-DMSO) δ: 6.80 (bs, 2H), 6.95 (bs, 2H), 7.30 (d, J = 8.6 Hz, 2H), 7.92 (d, J = 8.6 Hz, 2H), 10.4 (bs, 1H). MS (ESI): $[M+1]^+ = 213.19$.

5.1.2.9. 2-(3-Chlorobenzoyl)hydrazinecarboximidamide (7i). Synthesized according to method **A**, compound **7i** was obtained as a yellow solid (yield 38%); mp 163–165 °C. ^{1}H NMR (d_6-DMSO) δ: 6.77 (bs, 2H), 6.97 (bs, 2H), 7.29 (m, 2H), 7.86 (t, J = 7.2 Hz, 1H), 7.97 (s, 1H), 10.4 (s, 1H). MS (ESI): $[M+1]^+ = 213.31$.

5.1.2.10. 2-(4-Bromobenzoyl)hydrazinecarboximidamide (7j). Synthesized according to method **A**, compound **7j** was obtained as a yellow solid (yield 41%); mp 199–201 °C. ^{1}H NMR (d_6-DMSO) δ: 6.76 (bs, 2H), 6.91 (bs, 2H), 7.43 (d, J = 7.8 Hz, 2H), 7.86 (d, J = 7.8 Hz, 2H), 10.4 (bs, 1H). MS (ESI): $[M]^+ = 257.16$ and 259.26.

5.1.2.11. 2-(4-Methylbenzoyl)hydrazinecarboximidamide (7k). Synthesized according to method **A**, compound **7 k** was obtained as a white solid (yield 64%); mp 179–181 °C. ^{1}H NMR (d_6-DMSO) δ: 2.30 (s, 3H), 6.97 (bs, 4H), 7.10 (d, J = 8.0 Hz, 2H), 7.79 (s, 2H), 10,.3 (bs, 1H). MS (ESI): $[M+1]^+ = 193.25$.

5.1.2.12. 2-(3-Methylbenzoyl)hydrazinecarboximidamide (7l). Synthesized according to method **A**, compound **7l** was obtained as a pink solid (yield 67%); mp 161–162 °C. ^{1}H NMR (d_6-DMSO) δ: 2.31 (s, 3H), 7.08 (bs, 4H), 7.15 (m, 2H), 7.63 (t, J = 7.6 Hz, 1H), 7.77 (s, 1H), 10.1 (bs, 1H), 7.84 (bs, 2H). MS (ESI): $[M+1]^+ = 193.25$.

5.1.2.13. 2-(2-Methylbenzoyl)hydrazinecarboximidamide (7m). Synthesized according to method **A**, compound **7m** was obtained as a white solid (yield 52%); mp 105–107 °C. ^{1}H NMR (d_6-DMSO) δ: 6.57 (bs, 2H), 6.72 (bs, 2H), 7.11 (d, J = 7.4 Hz, 1H), 7.26 (m, 2H), 7.42 (d, J = 7.4 Hz, 1H), 10.1 (bs, 1H). MS (ESI): $[M+1]^+ = 193.25$.

5.1.2.14. 2-(4-Ethylbenzoyl)hydrazinecarboximidamide (7n). Synthesized according to method **A**, compound **7n** was obtained as a yellow solid (yield 43%); mp 170–171 °C. ^{1}H NMR (d_6-DMSO) δ: 1.14 (t, J = 7.4 Hz, 3H), 2.58 (q, J = 7.4 Hz, 2H), 6.92 (bs, 4H), 7.10 (d, J = 8.0 Hz, 2H), 7.81 (d, J = 8.0 Hz, 2H), 10.4 (bs, 1H). MS (ESI): [M+1]$^+$ = 207.24.

5.1.2.15. 2-(4-Methoxybenzoyl)hydrazinecarboximidamide (7o). Synthesized according to method **A**, compound **7o** was obtained as a yellow solid (yield 45%); mp 183–185 °C. ^{1}H NMR (d_6-DMSO) δ: 3.73 (s, 3H), 6.78 (bs, 4H), 6.84 (d, J = 8.8 Hz, 2H), 7.81 (d, J = 8.8 Hz, 2H), 10.3 (bs, 1H). MS (ESI): [M+1]$^+$ = 209.22.

5.1.2.16. 2-(3-Methoxybenzoyl)hydrazinecarboximidamide (7p). Synthesized according to method **A**, compound **7p** was obtained as a white solid (yield 45%); mp 169–171 °C. ^{1}H NMR (d_6-DMSO) δ: 3.76 (s, 3H), 6.80 (bs, 3H), 6.84 (bs, 2H), 7.17 (t, J = 8.0 Hz, 1H), 7.49 (s, 1H), 7.54 (d, J = 8.0 Hz, 1H), 10.4 (bs, 1H). MS (ESI): [M+1]$^+$ = 209.10.

5.1.2.17. 2-(4-Ethoxybenzoyl)hydrazinecarboximidamide (7q). Synthesized according to method **A**, compound **7q** was obtained as a white solid (yield 48%); mp 150–152 °C. ^{1}H NMR (d_6-DMSO) δ: 1.29 (t, J = 6.8 Hz, 3H), 4.01 (q, J = 6.8 Hz, 2H), 6.79 (d, J = 8.8 Hz, 2H), 6.88 (bs 2H), 7.82 (bs, 2H), 7.82 (d, J = 8.8 Hz, 2H), 10.4 (bs, 1H). MS (ESI): [M+1]$^+$ = 223.09.

5.1.2.18. 2-(4-Cyanobenzoyl)hydrazinecarboximidamide (7r). Synthesized according to method **A**, compound **7r** was obtained as a yellow solid (yield 63%); mp 163–165 °C. ^{1}H NMR (d_6-DMSO) δ: 6.87 (bs, 2H), 7.07 (bs, 2H), 7.73 (d, J = 8.0 Hz, 2H), 8.14 (d, J = 8.0 Hz, 2H), 10.2 (bs, 1H). MS (ESI): [M+1]$^+$ = 204.27.

5.1.2.19. 2-(3-Cyanobenzoyl)hydrazinecarboximidamide (7s). Synthesized according to method **A**, compound **7s** was obtained as a yellow solid (yield 54%); mp 182–184 °C. ^{1}H NMR (d_6-DMSO) δ: 6.66 (bs, 2H), 7.04 (bs, 2H), 7.49 (t, J = 7.4 Hz, 1H), 7.68 (d, J = 7.4 Hz, 1H), 8.02 (d, J = 7.4 Hz, 1H), 8.39 (s, 1H), 10.1 (bs, 1H). MS (ESI): [M+1]$^+$ = 204.27.

5.1.2.20. 2-(4-Nitrobenzoyl)hydrazinecarboximidamide (7t). Synthesized according to method **A**, compound **7t** was obtained as a red solid (yield 56%); mp 163–165 °C. ^{1}H NMR (d_6-DMSO) δ: 6.62 (bs, 2H), 7.22 (bs, 2H), 8.14 (d, J = 8.8 Hz, 2H), 8.23 (d, J = 8.8 Hz, 2H), 10.2 (bs, 1H). MS (ESI): [M]$^+$ = 224.21.

5.1.3. General method B for the preparation of compounds 8a-t.
A stirred suspension of the appropriate aryl/heteroaryl aminoguanidine **7a-t** (1 mmol) in water (5 mL) was placed in a 10 mL closed vial. The vessel was introduced into the microwave cavity (Pmax = 250 psi) using a CEM Discover microwave apparatus. Starting microwave irradiation of 100 W was used, the temperature being ramped from 25 to 100 °C in 2 min, with rapid stirring and venting. Once 100 °C was reached, the reaction mixture was held at this temperature for 10 min (Power: 100 W). After cooling, the precipitated product was filtered, washed with cold water and dried over P$_2$O$_5$, to furnish the appropriate 3-aryl-/heteroaryl-5-amino-1*H*-1,2,4-triazole derivatives **8a-t**. For the characterization of compound **8a-h**, **8k** and **8o**, see reference [41]. In addition, compounds **8i** [30] and **8j** [42] have shown to possess spectroscopic and analytical data as previously reported.

5.1.3.1. 3-(3-Tolyl)-1H-1,2,4-triazole-5-amine (8l). Synthesized according to method **B**, compound **8l** was obtained as a white solid (yield 63%); mp 167–168 °C. ^{1}H NMR (d_6-DMSO) δ: 2.33 (s, 3H), 6.03 (bs, 2H), 7.12 (d, J = 7.0 Hz, 1H), 7.23 (t, J = 7.0 Hz, 1H), 7.65 (m, 2H), 12.0 (bs, 1H). ^{13}C NMR (d_6-DMSO) δ: 20.97, 122.39, 125.83, 128.14, 128.63, 132.18, 137.22, 157.10, 158.33. MS (ESI): [M+1]$^+$ = 175.29.

5.1.3.2. 3-(2-Tolyl)-1H-1,2,4-triazole-5-amine (8m). Synthesized according to method **B**, compound **8m** was obtained as a white solid (yield 75%); mp 194–195 °C. ^{1}H NMR (d_6-DMSO) δ: 2.48 (s, 3H), 6.01 (bs, 2H), 7.23 (m, 3H), 7.82 (d, 1H), 12.1 (bs, 1H). ^{13}C NMR (d_6-DMSO) δ: 21.85, 125.34, 127.56, 128.46, 130.79, 131.22, 135.68, 156.38, 159.23. MS (ESI): [M+1]$^+$ = 175.29.

5.1.3.3. 3-(4-Ethyphenyl)-1H-1,2,4-triazol-5-amine (8n). Synthesized according to method **B**, compound **8n** was obtained as a yellow solid (yield 54%); mp 213–215 °C. ^{1}H NMR (d_6-DMSO) δ: 1.16 (t, J = 7.6 Hz, 3H), 2.57 (q, J = 7.6 Hz, 2H), 5.95 (bs, 2H), 7.18 (d, J = 7.8 Hz, 2H), 7.38 (d, J = 7.8 Hz, 2H), 12.1 (bs, 1H). ^{13}C NMR (d_6-DMSO) δ: 15.37, 27.87, 125.26 (2C), 126.43, 127.17, 127.68 (2C), 143.71, 158.86. MS (ESI): [M+1]$^+$ = 189.28.

5.1.3.4. 3-(3-Methoxyphenyl)-1H-1,2,4-triazol-5-amine (8p). Synthesized according to method **B**, compound **8p** was obtained as a white solid (yield 70%); mp 178–179 °C. ^{1}H NMR (d_6-DMSO) δ: 3.78 (s, 3H), 6.06 (bs, 2H), 6.92 (d, J = 7.2 Hz, 1H), 7.31 (t, J = 7.2 Hz, 1H), 7.45 (m, 2H), 12.1 (bs, 1H). ^{13}C NMR (d_6-DMSO) δ: 54.95, 110.41, 114.51, 117.68, 126.54, 129.58, 131.40, 133.56, 159.22. MS (ESI): [M+1]$^+$ = 191.02.

5.1.3.5. 3-(4-Ethoxyphenyl)-1H-1,2,4-triazol-5-amine (8q). Synthesized according to method **B**, compound **8q** was obtained as a white solid (yield 78%); mp 212–214 °C. ^{1}H NMR (d_6-DMSO) δ: 1.33 (t, J = 6.8 Hz, 3H), 4.03 (q, J = 6.8 Hz, 2H), 5.89 (bs, 2H), 6.92 (d, J = 8.0 Hz, 2H), 7.76 (d, J = 8.0 Hz, 2H), 12.0 (bs, 1H). ^{13}C NMR (d_6-DMSO) δ: 14.55, 63.90, 114.15 (2C), 122.56, 126.63 (2C), 141.68, 158.60, 159.56. MS (ESI): [M+1]$^+$ = 205.26.

5.1.3.6. 4-(5-Amino-1H-1,2,4-triazol-3-yl)benzonitrile (8r). Synthesized according to method **B**, compound **8r** was obtained as a yellow solid (yield 56%); mp 282–284 °C. ^{1}H NMR (d_6-DMSO) δ: 6.20 (bs, 2H), 7.83 (d, J = 8.6 Hz, 2H), 8.01 (d, J = 8.6 Hz, 2H), 12.3 (s, 1H). ^{13}C NMR (d_6-DMSO) δ: 110.34, 118.87, 125.75 (2C), 128.91, 132.51 (2C), 136.50, 157.62. MS (ESI): [M+1]$^+$ = 186.19.

5.1.3.7. 3-(5-Amino-1H-1,2,4-triazol-3-yl)benzonitrile (8s). Synthesized according to method **B**, compound **8s** was obtained as a white solid (yield 58%); mp 227–229 °C. ^{1}H NMR (d_6-DMSO) δ: 6.19 (bs, 2H), 7.62 (t, J = 7.8 Hz, 1H), 7.79 (d, J = 7.8 Hz, 1H), 8.15 (s, 1H), 8.19 (d, J = 7.8 Hz, 1H), 12.3 (s, 1H). ^{13}C NMR (d_6-DMSO) δ: 111.57, 118.61, 128.30, 129.66, 129.86, 131.64, 133.40, 156.60, 157.53. MS (ESI): [M+1]$^+$ = 186.31.

5.1.3.8. 3-(4-Nitrophenyl)-1H-1,2,4-triazol-5-amine (8t). Synthesized according to method **B**, compound **8t** was obtained as an orange solid (yield 45%); mp 274–276 °C. ^{1}H NMR (d_6-DMSO) δ: 6.24 (bs, 2H), 8.08 (d, J = 8.8 Hz, 2H), 8.25 (d, J = 8.8 Hz, 2H), 12.4 (bs, 1H). ^{13}C NMR (d_6-DMSO) δ: 123.90 (2C). 126.06 (2C), 128.26, 138.36, 146.89, 157.73. MS (ESI): [M+1]$^+$ = 206.13.

5.1.4. General method C for the synthesis of compounds 5a-v
To a stirred solution of the appropriate 1,2,4-triazole **8a-t** (1 mmol) in dry pyridine (5 mL) cooled at −5 °C was added 3′,4′,5′-trimethoxybenzoyl chloride (252 mg, 1.1 mol, 1.1 equiv.) in small portions. For the preparation of compounds **5u** and **5v**, 3′,4′-dimethoxybenzoyl chloride (221 mg, 1.1 mmol, 1.1 equiv.) or 4′-methoxybenzoyl chloride (188 mg, 1.1 mmol, 1.1 equiv.), respectively, were added to derivative **5k**. The reaction mixture was kept for 30 min at −5 °C and then overnight at room temperature. Pyridine was removed by evaporation under reduced pressure. To the residue was added CH$_2$Cl$_2$, and the organic phase was washed with saturated aq. NaHCO$_3$, water and brine and dried. The reaction mixture was filtered, and the solvent was removed *in vacuo*. The crude residue was suspended in ethyl ether (15 mL), the resulting suspension stirred for 30 min, filtered and the residue filtered under reduced pressure to furnish the 1-aroyl-3-aryl-5-

amino-1*H*-1,2,4-triazole derivatives **5a-v**. Compounds **5a**, **5e**, **5f** and **5h** were characterized by spectroscopic and analytical data, and our data were in agreement with those previously reported [30].

5.1.4.1. (5-Amino-3-phenyl-1H-1,2,4-triazol-1-yl) (3,4,5-trimethoxyphenyl) methanone (5a). Synthesized according to method **C**, derivative **5a** was obtained as a white solid (yield 66%); mp 225–227 °C. ^{1}H NMR (d_6-DMSO) δ: 3.80 (s, 3H), 3.87 (s, 6H), 7.47 (m, 3H), 7.68 (s, 2H), 7.86 (bs, 2H), 8.03 (m, 2H). ^{13}C NMR (d_6-DMSO) δ: 55.96 (2C), 60.13, 108.92 (2C), 126.22 (2C), 126.42, 128.70 (2C), 130.02, 130.64, 141.60, 152.00 (2C), 159.05, 159.40, 166.39. MS (ESI): $[M+1]^+ = 355.37$. Anal. calcd for $C_{18}H_{18}N_4O_4$. C, 61.01; H, 5.12; N, 15.81; found: C, 60.78; H, 5.01; N, 15.67.

5.1.4.2. (5-Amino-3-(thiophen-2-yl)-1H-1,2,4-triazol-1-yl) (3,4,5-trimethoxyphenyl) methanone (5b). Synthesized according to method **C**, derivative **5b** was obtained as a white solid (yield 42%); mp 190–192 °C. ^{1}H NMR (d_6-DMSO) δ: 3.78 (s, 3H), 3.88 (s, 6H), 7.18 (dd, J = 5.0 and 3.8 Hz, 1H), 7.63 (m, 3H), 7.64 (d, J = 3.8 Hz, 1H), 7.88 (bs, 2H). ^{13}C NMR (d_6-DMSO) δ: 55.99 (2C), 60.22, 109.05 (2C), 126.30, 127.56, 128.14, 128.60, 133.04, 141.69, 152.05 (2C), 155.89, 158.98, 166.12. MS (ESI): $[M+1]^+ = 361.19$. Anal. calcd for $C_{16}H_{16}N_4O_4S$. C, 53.32; H, 4.47; N, 15.55; found: C, 53.14; H, 4.29; N, 15.40.

5.1.4.3. (5-Amino-3-(furan-2-yl)-1H-1,2,4-triazol-1-yl) (3,4,5-trimethoxyphenyl) methanone (5c). Synthesized according to method **C**, derivative **5c** was obtained as a white solid (yield 54%); mp 212–214 °C. ^{1}H NMR (d_6-DMSO) δ: 3.79 (s, 3H), 3.84 (s, 6H), 6.64 (dd, J = 3.2 and 1.6 Hz, 1H), 6.98 (d, J = 3.2 Hz, 1H), 7.53 (m, 3H), 7.85 (bs, 2H). ^{13}C NMR (d_6-DMSO) δ: 56.00 (2C), 60.14, 108.78 (2C), 111.53, 111.76, 126.51, 141.54, 144.74, 145.43, 152.01 (2C), 152.75, 158.71, 166.53. MS (ESI): $[M+1]^+ = 345.12$. Anal. calcd for $C_{16}H_{16}N_4O_5$. C, 58.81; H, 4.68; N, 16.27; found: C, 58.69; H, 4.49; N, 16.19.

5.1.4.4. (5-Amino-3-(pyridin-2-yl)-1H-1,2,4-triazol-1-yl) (3,4,5-trimethoxyphenyl) methanone (5d). Synthesized according to method **C**, derivative **5d** was obtained as a white solid (yield 62%); mp 227–229 °C. ^{1}H NMR (d_6-DMSO) δ: 3.82 (s, 3H), 3.88 (s, 6H), 7.42 (dd, J = 5.2 and 1.6H Hz, 1H), 7.58 (s, 2H), 7.82 (bs, 2H), 7.88 (t, J = 5.2 Hz, 1H), 8.02 (d, J = 5.2 Hz, 1H), 8.63 (d, J = 1.6 Hz, 1H). ^{13}C NMR (d_6-DMSO) δ: 56.12 (2C), 60.23, 108.99 (2C), 122.32, 124.72, 126.61, 137.06, 141.71, 148.96, 149.80, 152.13 (2C), 159.08, 159.50, 166.94. MS (ESI): $[M+1]^+ = 356.48$. Anal. calcd for $C_{17}H_{17}N_5O_4$. C, 57.46; H, 4.82; N, 19.71; found: C, 57.31; H, 4.67; N, 19.58.

5.1.4.5. (5-Amino-3-(pyridin-3-yl)-1H-1,2,4-triazol-1-yl) (3,4,5-trimethoxyphenyl) methanone (5e). Synthesized according to method **C**, derivative **5e** was obtained as a white solid (yield 46%); mp 221–222 °C. ^{1}H NMR (d_6-DMSO) δ: 3.80 (s, 3H), 3.87 (s, 6H), 7.51 (t, J = 5.2 Hz, 1H), 7.61 (s, 2H), 7.94 (bs, 2H), 8.27 (d, J = 5.2 Hz, 1H), 8.66 (d, J = 5.2 Hz, 1H), 9.13 (s, 1H). ^{13}C NMR (d_6-DMSO) δ: 56.05 (2C), 60.20, 105.66, 108.97 (2C), 123.99, 126.02, 126.32, 133.67, 147.31, 150.88, 152.09 (2C), 157.52, 159.20, 166.46. MS (ESI): $[M+1]^+ = 356.36$. Anal. calcd for $C_{17}H_{17}N_5O_4$. C, 57.46; H, 4.82; N, 19.71; found: C, 57.21; H, 4.58; N, 19.39.

5.1.4.6. (5-Amino-3-(pyridin-4-yl)-1H-1,2,4-triazol-1-yl) (3,4,5-trimethoxyphenyl) methanone (5f). Synthesized according to method **C**, derivative **5f** was obtained as a white solid (yield 51%); mp 227–229 °C. ^{1}H NMR (d_6-DMSO) δ: 3.80 (s, 3H), 3.87 (s, 6H), 7.58 (s, 2H), 7.85 (dd, J = 4.4 and 1.6 Hz, 2H), 7.96 (bs, 2H), 8.68 (m, 2H). ^{13}C NMR (d_6-DMSO) δ: 56.11 (2C), 60.25, 105.71, 109.01 (2C), 119.75, 120.39, 126.28, 137.38, 150.37, 150.47, 152.13, 152.72, 157.71, 159.34, 166.61. MS (ESI): $[M+1]^+ = 356.36$. Anal. calcd for $C_{17}H_{17}N_5O_4$. C, 57.46; H, 4.82; N, 19.71; found: C, 57.32; H, 4.70; N, 19.63.

5.1.4.7. (5-Amino-3-(4-fluorophenyl)-1H-1,2,4-triazol-1-yl) (3,4,5-trimethoxyphenyl)methanone (5g). Synthesized according to method **C**, compound **5g** was obtained as a white solid (yield 64%); mp 248–250 °C. ^{1}H NMR (d_6-DMSO) δ: 3.79 (s, 3H), 3.86 (s, 6H), 7.32 (t, J = 6.8 Hz, 2H), 7.60 (s, 2H), 7.88 (bs, 2H), 8.01 (t, J = 6.8 Hz, 2H). ^{13}C NMR (d_6-DMSO) δ: 55.98 (2C), 60.14, 108.87 (2C), 115.66 (J = 85.2 Hz), 126.42, 126,60, 128.48, 128.57, 141.59, 152.01 (2C), 158.61, 159.09, 161.91, 164.36, 166.43. MS (ESI): $[M+1]^+ = 373.2$. Anal. calcd for $C_{18}H_{17}FN_4O_4$. C, 58.06; H, 4.60; N, 15.05; found: C, 57.93; H, 4.46; N, 14.89.

5.1.4.8. (5-Amino-3-(4-chlorophenyl)-1H-1,2,4-triazol-1-yl) (3,4,5-trimethoxyphenyl) methanone (5h). Synthesized according to method **C**, compound **5h** was obtained as a white solid (yield 51%); mp 217–219 °C. ^{1}H NMR (d_6-DMSO) δ: 3.78 (s, 3H), 3.86 (s, 6H), 7.52 (d, J = 8.8 Hz, 2H), 7.56 (s, 2H), 7.86 (bs, 2H), 7.94 (d, J = 8.8 Hz, 2H). ^{13}C NMR (d_6-DMSO) δ: 55.97 (2C), 60.15, 108.86 (2C), 126.39, 127.97 (2C), 128.88 (2C), 134.64 (2C), 141.60, 152.01 (2C), 158.49, 159.09, 166.45. MS (ESI): $[M+1]^+ = 389.3$. Anal. calcd for $C_{18}H_{17}ClN_4O_4$. C, 55.60; H, 4.41; N, 14.41; found: C, 55.38; H, 4.29; N, 14.30.

5.1.4.9. (5-Amino-3-(3-chlorophenyl)-1H-1,2,4-triazol-1-yl) (3,4,5-trimethoxyphenyl) methanone (5i). Synthesized according to method **C**, compound **5i** was obtained as a white solid (yield 59%); mp 239–241 °C. ^{1}H NMR (d_6-DMSO) δ: 3.80 (s, 3H), 3.87 (s, 6H), 7.54 (m, 2H), 7.60 (s, 2H), 7.91 (m, 4H). ^{13}C NMR (d_6-DMSO) δ: 55.95 (2C), 60.15, 108.92 (2C), 124.73, 125.80, 126.28, 129.81, 130.84, 132.14, 133.36, 141.66, 152.00 (2C), 158.13, 159.10, 166.40. MS (ESI): $[M+1]^+ = 389.43$. Anal. calcd for $C_{18}H_{17}ClN_4O_4$. C, 55.60; H, 4.41; N, 14.41; found: C, 55.42; H, 4.30; N, 14.28.

5.1.4.10. (5-Amino-3-(4-bromophenyl)-1H-1,2,4-triazol-1-yl) (3,4,5-trimethoxyphenyl) methanone (5j). Synthesized according to method **C**, compound **5j** was obtained as a white solid (yield 59%); mp 219–220 °C. ^{1}H NMR (d_6-DMSO) δ: 3.80 (s, 3H), 3.86 (s, 6H), 7.58 (s, 2H), 7.70 (d, J = 8.4 Hz, 2H), 7.86 (bs, 2H), 7.88 (d, J = 8.4 Hz, 2H). ^{13}C NMR (d_6-DMSO) δ: 56.08 (2C), 60.23, 108.96 (2C), 123.51, 126.47, 128.30 (2C), 129.38, 131.88 (2C), 141.70, 152.10 (2C), 158.66, 159.17, 166.53. MS (ESI): $[M]^+ = 433.27$ and 435.38. Anal. calcd for $C_{18}H_{17}BrN_4O_4$. C, 49.90; H, 3.95; N, 12.93; found: C, 49.77; H, 3.78; N, 12.81.

5.1.4.11. (5-Amino-3-(p-tolyl)-1H-1,2,4-triazol-1-yl) (3,4,5-trimethoxyphenyl) methanone (5k). Synthesized according to method **C**, compound **5k** was obtained as a white solid (yield 42%); mp 208–209 °C. ^{1}H NMR (d_6-DMSO) δ: 2.33 (s, 3H), 3.78 (s, 3H), 3.84 (s, 6H), 7.26 (d, J = 8.0 Hz, 2H), 7.60 (s, 2H), 7.81 (bs, 2H), 7.83 (d, J = 8.0 Hz, 2H). ^{13}C NMR (d_6-DMSO) δ: 21.02, 56.04 (2C), 60.23, 108.99 (2C), 126.28 (2C), 126.57, 127.40, 129.37 (2C), 139.79, 141.65, 152.08 (2C), 159.08, 159.56, 166.45. MS (ESI): $[M+1]^+ = 369.49$. Anal. calcd for $C_{19}H_{20}N_4O_4$. C, 61.95; H, 5.47; N, 15.21; found: C, 61.81; H, 5.35; N, 15.01.

5.1.4.12. (5-Amino-3-(m-tolyl)-1H-1,2,4-triazol-1-yl) (3,4,5-trimethoxyphenyl) methanone (5l). Synthesized according to method **C**, compound **5l** was obtained as a white solid (yield 54%); mp 216–218 °C. ^{1}H NMR (d_6-DMSO) δ: 2.36 (s, 3H), 3.80 (s, 3H), 3.87 (s, 6H), 7.29 (d, J = 7.6 Hz, 1H), 7.35 (t, J = 7.6 Hz, 1H), 7.64 (s, 2H), 7.71 (d, J = 7.6 Hz, 1H), 7.80 (s, 1H), 7.84 (bs, 2H). ^{13}C NMR (d_6-DMSO) δ: 20.92, 55.93 (2C), 60.14, 108.95 (2C), 123.40, 126.41, 126.78, 128.61, 129.99, 130.66, 137.81, 141.61, 151.99 (2C), 159.00, 159.48, 166.33. MS (ESI): $[M+1]^+ = 369.36$. Anal. calcd for $C_{19}H_{20}N_4O_4$. C, 61.95; H, 5.47; N, 15.21; found: C, 61.79; H, 5.38; N,

15.05.

5.1.4.13. (5-Amino-3-(o-tolyl)-1H-1,2,4-triazol-1-yl)(3,4,5-trimethoxyphenyl) methanone (5m). Synthesized according to method **C**, compound **5m** was obtained as a white solid (yield 75%); mp 193–195 °C. ^{1}H NMR (d_6-DMSO) δ: 2.62 (s, 3H), 3.78 (s, 3H), 3.86 (s, 6H), 7.25 (m, 3H), 7.58 (s, 2H), 7.82 (bs, 2H), 8.00 (d, $J = 7.6$ Hz, 1H). ^{13}C NMR (d_6-DMSO) δ: 22.23, 56.07 (2C), 60.23, 108.85 (2C), 125.85, 126.79, 128.98, 129.44 (2C), 131.23, 136.82, 141.71, 152.10 (2C), 158.23, 160.41, 166.70. MS (ESI): $[M+1]^+ = 369.24$. Anal. ($C_{19}H_{20}N_4O_4$) C, H, N. Anal. calcd for $C_{19}H_{20}N_4O_4$. C, 61.95; H, 5.47; N, 15.21; found: C, 61.77; H, 5.29; N, 15.05.

5.1.4.14. (5-Amino-3-(4-ethylphenyl)-1H-1,2,4-triazol-1-yl) (3,4,5-trimethoxyphenyl) methanone (5n). Synthesized according to method **C**, compound **5n** was obtained as a white solid (yield 52%); mp 171–173 °C. ^{1}H NMR (d_6-DMSO) δ: 1.20 (t, $J = 7.6$ Hz, 3H), 2.64 (q, $J = 7.6$ Hz, 2H), 3.80 (s, 3H), 3.86 (s, 6H), 7.31 (d, $J = 8.0$ Hz, 2H), 7.63 (s, 2H), 7.82 (bs, 2H), 7.88 (d, $J = 8.0$ Hz, 2H). ^{13}C NMR (d_6-DMSO) δ: 15.25, 27.98, 55.96 (2C), 60.15, 108.92 (2C), 126.29 (2C), 126.46, 127.56, 128.10 (2C), 141.56, 145.92, 151.99 (2C), 159.00, 159.48, 166.33. MS (ESI): $[M+1]^+ = 383.48$. Anal. calcd for $C_{20}H_{22}N_4O_4$. C, 62.82; H, 5.80; N, 14.65; found: C, 62.71; H, 5.69; N, 14.52.

5.1.4.15. (5-Amino-3-(4-methoxyphenyl)-1H-1,2,4-triazol-1-yl) (3,4,5-trimethoxyphenyl) methanone (5o). Synthesized according to method **C**, compound **5o** was obtained as a white solid (yield 66%); mp 206–208 °C. ^{1}H NMR (d_6-DMSO) δ: 3.79 (s, 3H), 3.80 (s, 3H), 3.87 (s, 6H), 7.03 (d, $J = 9.2$ Hz, 2H), 7.63 (s, 2H), 7.83 (bs, 2H), 7.90 (d, $J = 9.2$ Hz, 2H). ^{13}C NMR (d_6-DMSO) δ: 55.14, 55.95 (2C), 60.12, 108.91 (2C), 114.10 (2C), 122.47, 126.51, 127.81 (2C), 141.53, 151.98 (2C), 158.98, 159.12, 160.68, 166.27. MS (ESI): $[M+1]^+ = 385.22$. Anal. calcd for $C_{19}H_{20}N_4O_5$. C, 59.37; H, 5.24; N, 14.58; found: C, 59.25; H, 5.11; N, 14.47.

5.1.4.16. (5-Amino-3-(3-methoxyphenyl)-1H-1,2,4-triazol-1-yl) (3,4,5-trimethoxyphenyl) methanone (5p). Synthesized according to method **C**, compound **5p** was obtained as a white solid (yield 69%); mp 199–200 °C. ^{1}H NMR (d_6-DMSO) δ: 3.80 (s, 3H), 3.81 (s, 3H), 3.87 (s, 6H), 7.03 (m, 1H), 7.40 (t, $J = 8.0$ Hz, 1H), 7.49 (d, $J = 1.6$ Hz, 1H), 7.56 (m, 1H), 7.66 (s, 2H), 7.87 (bs, 2H). ^{13}C NMR (d_6-DMSO) δ: 54.95, 55.93 (2C), 60.16, 109.01 (2C), 110.92, 116.10, 118.58, 126.32, 129.92 (2C), 131.40, 141.66, 152.01 (2C), 159.06, 159.28, 166.26. MS (ESI): $[M+1]^+ = 385.34$. Anal. calcd for $C_{19}H_{20}N_4O_5$. C, 59.37; H, 5.24; N, 14.58; found: C, 59.28; H, 5.09; N, 14.40.

5.1.4.17. (5-Amino-3-(4-ethoxyphenyl)-1H-1,2,4-triazol-1-yl) (3,4,5-trimethoxyphenyl) methanone (5q). Synthesized according to method **C**, compound **5q** was obtained as a white solid (yield 69%); mp 196–198 °C. ^{1}H NMR (d_6-DMSO) δ: 1.34 (t, $J = 7.2$ Hz, 3H), 3.79 (s, 3H), 3.86 (s, 6H), 4.06 (q, $J = 7.2$ Hz, 2H), 7.00 (d, $J = 8.8$ Hz, 2H), 7.62 (s, 2H), 7.82 (bs, 2H), 7.88 (d, $J = 8.8$ Hz, 2H). ^{13}C NMR (d_6-DMSO) δ: 14.50, 55.95 (2C), 60.12, 63.08, 108.89 (2C), 114.50 (2C), 122.31, 126.53, 127.81 (2C), 141.52, 151.98 (2C), 158.97, 159.35, 159.97, 166.29. MS (ESI): $[M+1]^+ = 399.46$. Anal. calcd for $C_{20}H_{22}N_4O_5$. C, 60.29; H, 5.57; N, 14.06; found: C, 60.12; H, 5.39; N, 13.89.

5.1.4.18. 4-(5-Amino-1-(3,4,5-trimethoxybenzoyl)-1H-1,2,4-triazol-3-yl) benzonitrile (5r). Synthesized according to method **C**, compound **5r** was obtained as a yellow solid (yield 63%); mp 248–250 °C. ^{1}H NMR (d_6-DMSO) δ: 3.80 (s, 3H), 3.86 (s, 6H), 7.57 (s, 2H), 7.94 (bs, 2H), 7.96 (d, $J = 8.0$ Hz, 2H), 8.10 (d, $J = 8.0$ Hz, 2H). ^{13}C NMR (d_6-DMSO) δ: 55.99 (2C), 60.14, 108.86 (2C), 112.21, 118.48, 126.25, 126.86 (2C), 132.80 (2C), 134.35, 141.68, 152.01 (2C), 157.96, 159.17, 166.52. MS (ESI):

$[M]^+ = 380.28$. Anal. calcd for $C_{19}H_{17}N_5O_4$. C, 60.14; H, 4.52; N, 18.46; found: C, 60.01; H, 4.37; N, 18.29.

5.1.4.19. 3-(5-amino-1-(3,4,5-trimethoxybenzoyl)-1H-1,2,4-triazol-3-yl) benzonitrile (5s). Synthesized according to method **C**, compound **5s** was obtained as a white solid (yield 92%); mp 185–187 °C. ^{1}H NMR (d_6-DMSO) δ: 3.80 (s, 3H), 3.87 (s, 6H), 7.58 (s, 2H), 7.72 (t, $J = 7.8$ Hz, 1H), 7.94 (m, 3H), 8.24 (m, 2H). ^{13}C NMR (d_6-DMSO) δ: 56.52 (2C), 60.69, 109.42 (2C), 112.46, 118.81, 126.80, 129.62, 130.03, 130.72, 131.19, 131.84, 134.06, 142.23, 152.58, 158.26, 159.72, 167.04. MS (ESI): $[M+1]^+ = 380.26$. Anal. calcd for $C_{19}H_{17}N_5O_4$. C, 60.14; H, 4.52; N, 18.46; found: C, 60.00; H, 4.40; N, 18.31.

5.1.4.20. (5-Amino-3-(4-nitrophenyl)-1H-1,2,4-triazol-1-yl) (3,4,5-trimethoxyphenyl) methanone (5t). Synthesized according to method **C**, compound **5t** was obtained as a yellow solid (yield 40%); mp 218–220 °C. ^{1}H NMR (d_6-DMSO) δ: 3.82 (s, 3H), 3.87 (s, 6H), 7.58 (s, 2H), 7.95 (bs, 2H), 8.18 (d, $J = 8.8$ Hz, 2H), 8.33 (d, $J = 8.8$ Hz, 2H). ^{13}C NMR (d_6-DMSO) δ: 56.57 (2C), 60.70, 109.40 (2C), 124.68 (2C), 126.80, 127.92 (2C), 136.65, 142.22, 148.66, 152.58 (2C), 158.26, 159.78, 167.11. MS (ESI): $[M]^+ = 400.33$. Anal. calcd for $C_{18}H_{17}N_5O_6$. C, 54.14; H, 4.29; N, 17.54; found: C, 54.01; H, 4.12; N, 17.38.

5.1.4.21. (5-Amino-3-(p-tolyl)-1H-1,2,4-triazol-1-yl)(3,4-dimethoxyphenyl) methanone (5u). Synthesized according to method **C**, compound **5u** was obtained as a white solid (yield 55%); mp 201–203 °C. ^{1}H NMR (d_6-DMSO) δ: 2.32 (s, 3H), 3.80 (s, 3H), 3.84 (s, 3H), 7.14 (d, $J = 8.0$ Hz, 1H), 7.30 (d, $J = 8.0$ Hz, 2H), 7.78 (bs, 2H), 7.92 (m, 3H), 8.05 (d, $J = 8.0$ Hz, 1H). ^{13}C NMR (d_6-DMSO) δ: 21.02, 55.51, 55.79, 110.75 (2C), 114.17, 123.57, 125.99, 126.31, 127.48, 129.31 (2C), 139.72, 147.77, 153.05, 159.11, 159.43, 166.36. MS (ESI): $[M+1]^+ = 339.52$. Anal. calcd for $C_{18}H_{18}N_4O_3$. C, 63.89; H, 5.36; N, 16.56; found: C, 63.78; H, 5.22; N, 16.45.

5.1.4.22. (5-Amino-3-(p-tolyl)-1H-1,2,4-triazol-1-yl)(4-methoxyphenyl) methanone (5v). Synthesized according to method **C**, compound **5v** was obtained as a white solid (yield 50%); mp 180–182 °C. ^{1}H NMR (d_6-DMSO) δ: 2.33 (s, 3H), 3.86 (s, 3H), 7.09 (dd, $J = 8.8$ and 2.4 Hz, 2H), 7.28 (d, $J = 8.4$ Hz, 2H), 7.76 (bs, 2H), 7.84 (d, $J = 8.4$ Hz, 2H), 8.24 (dd, $J = 8.8$ and 2.4 Hz, 2H). ^{13}C NMR (d_6-DMSO) δ: 21.03, 55.60, 113.56 (2C), 123.83, 126.37 (2C), 127.46, 129.25 (2C), 133.63 (2C), 139.71, 159.04, 159.46, 163.14, 166.49. MS (ESI): $[M+1]^+ = 309.54$. Anal. calcd for $C_{17}H_{16}N_4O_2$. C, 66.22; H, 5.23; N, 18.17; found: C, 66.12; H, 5.08; N, 18.02.

5.2. Biological assays and computational studies

5.2.1. Cell growth conditions and antiproliferative assay

Human *T*-leukemia (Jurkat) and human B-leukemia (RS4;11) cells were grown in RPMI-1640 medium (Gibco, Milano, Italy). Breast adenocarcinoma (MCF-7), human cervix carcinoma (HeLa), and human colon adenocarcinoma (HT-29) cells were grown in DMEM medium (Gibco, Milano, Italy), all supplemented with 115 units/mL penicillin G (Gibco, Milano, Italy), 115 µg/mL streptomycin (Invitrogen, Milano, Italy), and 10% fetal bovine serum (Invitrogen, Milano, Italy). Stock solutions (10 mM) of the different compounds were obtained by dissolving them in DMSO. Individual wells of a 96-well tissue culture microtiter plate were inoculated with 100 µL of complete medium containing 8×10^3 cells. The plates were incubated at 37 °C in a humidified 5% CO_2 incubator overnight prior to the experiments. After medium removal, 100 µL of fresh medium containing the test compound at different concentrations was added to each well in triplicate and incubated at 37 °C for 72 h. Cell viability was assayed by the (3-(4, 5-dimethylthiazol-2-yl)-2,5-diphenyltetrazolium bromide test as previously described [43].

5.2.2. Effects on tubulin polymerization and on colchicine binding to tubulin.

Bovine brain tubulin was purified as described previously [44]. To evaluate the effect of the compounds on tubulin assembly *in vitro* [45], varying concentrations were preincubated with $10\,\mu M$ tubulin in glutamate buffer at $30\,°C$ and then cooled to $0\,°C$. After addition of GTP, the mixtures were transferred to $0\,°C$ cuvettes in a recording spectrophotometer and warmed to $30\,°C$, and the assembly of tubulin was observed turbidimetrically. The IC_{50} was defined as the compound concentration that inhibited the extent of assembly by 50% after a 20 min incubation. The capacity of the test compounds to inhibit colchicine binding to tubulin was measured as described [46], except that the reaction mixtures contained $1\,\mu M$ tubulin, $5\,\mu M$ [^{3}H]colchicine and $5\,\mu M$ test compound.

5.2.3. Molecular modeling

All molecular docking studies were performed on a Viglen Genie Intel®Core^{TM} i7-3770 vPro CPU@ 3.40 GHz × 8 running Ubuntu 14.04. Molecular Operating Environment (MOE) 2015.10 and Maestro (Schrödinger Release 2017-1) were used as molecular modeling software. The tubulin structures were downloaded from the PDB data bank (http://www.rcsb.org/; PDB code 4O2B, 3N2G). The proteins were preprocessed using the Schrödinger Protein Preparation Wizard by assigning bond orders, adding hydrogens and performing a restrained energy minimization of the added hydrogens using the OPLS_2005 force field. Ligand structures were built with MOE and then prepared using the Maestro LigPrep tool by energy minimizing the structures (OPLS_2005 force filed), generating possible ionization states at pH 7 ± 2, generating tautomers and low-energy ring conformers. After isolating a tubulin dimer structure, two $12\,\text{Å}$ docking grids (inner-box $10\,\text{Å}$ and outer-box $22\,\text{Å}$) were prepared using as centroid the co-crystallized colchicine in the 4O2B structure and the co-crystallized G2N in the 3N2G protein. Molecular docking studies were performed using Glide SP precision keeping the default parameters and setting 6 as number of output poses per input ligand to include in the solution. The output poses were then refined with Glide XP scoring and the output database saved as a mol2 file. The docking results were visually inspected for their ability to bind the active site. MD simulations were performed on Supermicro Intel®Xeon® CPU ES-46200 @ 2.20 GHz × 12 running Ubuntu 14.04 using the Desmond package for MD simulation: OPLS-AA force field in explicit solvent, employing the TIP3 water model was used. The initial coordinates for the MD simulation were taken from the best docking experiment result for each single compound. A cubic water box was used for the solvation of the system, ensuring a buffer distance of approximately $10\,\text{Å}$ between each box side and the complex atoms. The system was neutralized adding either 21 (4O2B) or 24 (3N2G) sodium counter ions. The system was minimized and pre-equilibrated using the default relaxation routine implemented in Desmond. A 20 ns MD simulation was performed, during which the equations of motion were integrated using a 2 fs time step in the NPT ensemble, with temperature (300 K) and pressure (1 atm) constant. All other parameters were set using the Desmond default values. Data were collected every 8 ps (energy) and every 32 ps (trajectory). Each protein-ligand complex simulation was performed in triplicate, using each time a random seed as starting point. Visualization of protein-ligand complex and MD trajectory analysis was carried out using Maestro, and the RMSD analyses were performed using the Simulation Event Analysis tool and the Simulation Interaction Diagram of Desmond. The $\Delta G_{\text{binding}}$ values of the protein-ligand complex were calculated using the MM/GBSA method as implemented in the Prime module from Maestro using the default settings and the Maestro script termal_mmgbsa.py. Briefly, the script takes in the MD trajectory from the last 14 ns of simulation, splits it into individual frame snapshots (extracted every 0.064 ns, for a total of 220 frames), and runs each one through MMGBSA (after deleting waters and separating the ligand from the receptor). For each single simulation, an average $\Delta G_{\text{binding}}$ value for the 14 ns is calculated.

5.2.4. Flow cytometric analysis of cell cycle distribution

5×10^5 HeLa cells were treated with different concentrations of the test compounds for 24 h. After the incubation period, the cells were collected, centrifuged, and fixed with ice-cold ethanol (70%). The cells were then treated with lysis buffer containing RNase A and 0.1% Triton X-100 and then stained with PI. Samples were analyzed on a Cytomic FC500 flow cytometer (Beckman Coulter). DNA histograms were analyzed using MultiCycle for Windows (Phoenix Flow Systems).

5.2.5. Apoptosis assay

Cell death was determined by flow cytometry of cells double stained with annexin V/FITC and PI. The Coulter Cytomics FC500 (Beckman Coulter) was used to measure the surface exposure of phosphatidyl serine on apoptotic cells according to the manufacturer's instructions (Annexin-V Fluos, Roche Diagnostics).

5.2.6. Statistical analysis

Unless indicated differently, the results are presented as mean ± S.E.M. The differences between different treatments were analyzed using the two-sided Student's *t* test. P values lower than 0.05 were considered significant.

Acknowledgment

Disclaimer

The content of this paper is solely the responsibility of the authors and does not necessarily reflect the official views of the National Institutes of Health.

Appendix A. Supplementary material

Supplementary data associated with this article can be found, in the online version, at https://doi.org/10.1016/j.bioorg.2018.06.037.

References

[1] A. Akhmanova, M.O. Steinmetz, Control of microtubule organization and dynamics: two ends in the limelight, Nat. Rev. Mol. Cell. Biol. 16 (2015) 711–726.

[2] T. Horio, T. Murata, The role of dynamic instability in microtubule organization, Front. Plant Sci. 5 (2014) 511.

[3] C. Janke, The tubulin code: molecular components, readout mechanisms, and functions, J. Cell Biol. 206 (2014) 461–472.

[4] A.L. Risinger, F.J. Giles, S.L. Mooberry, Microtubule dynamics as a target in oncology, Cancer Treat. Rev. 35 (2009) 255–261.

[5] N.G. Vindya, N. Sharma, M. Yadav, K.R. Ethiraj, Tubulins-the target for anticancer therapy, Curr. Top. Med. Chem. 15 (2015) 73–82.

[6] V. Nitika, K. Kapil, Microtubule targeting agents: a benchmark in cancer therapy, Curr. Drug Ther. 8 (2014) 189–196.

[7] C.C. Rohena, S.L. Mooberry, Recent progress with microtubule stabilizers: new compounds, binding modes and cellular activities, Nat. Prod. Rep. 31 (2014) 335–355.

[8] J. Seligmann, C. Twelves, Tubulin: an example of targeted chemotherapy, Future Med. Chem. 5 (2013) 339–352.

[9] C.D. Katsetos, P. Dráber, Tubulins as therapeutic targets in cancer: from bench to bedside, Curr. Pharm. Des. 18 (2012) 2778–2792.

[10] C. Dumontet, M.A. Jordan, Microtubule-binding agents: a dynamic field of cancer therapeutics, Nat. Rev. Drug. Discov. 9 (2010) 790–803.

[11] R.A. Stanton, K.M. Gernert, J.H. Nettles, R. Aneja, Drugs that target dynamic microtubules: a new molecular perspective, Med. Res. Rev. 31 (2011) 443–481.

[12] J.J. Field, A. Kanakkanthara, J.H. Miller, Microtubule-targeting agents are clinically successful due to both mitotic and interphase impairment of microtubule function, Bioorg. Med. Chem. 22 (2014) 5050–5059.

[13] Y.M. Liu, H.L. Chen, H.Y. Lee, J.P. Liou, Tubulin inhibitors: a patent review, Expert Opin. Ther. Pat. 24 (2014) 69–88.

[14] Y. Lu, J.J. Chen, M. Xiao, W. Li, D.D. Miller, An overview of tubulin inhibitors that interact with the colchicine binding site, Pharm. Res. 29 (2012) 2943–2971.

[15] R. Alvarez, M. Medarde, R. Pelaez, New ligands of the tubulin colchicine site based on X-ray structures, Curr. Top. Med. Chem. 14 (2014) 2231–2252.

[16] R.J. van Vuuren, M.H. Visagie, A.E. Theron, A.M. Joubert, Antimitotic drugs in the treatment of cancer, Cancer Chemother. Pharmacol. 76 (2015) 1101–1112.

[17] G.R. Pettit, S.B. Singh, E. Hamel, C.M. Lin, D.S. Alberts, D. Garcia-Kendall, Isolation

and structure of the strong cell growth and tubulin inhibitor combretastatin A-4, Experientia 45 (1989) 209–211.

[18] C.M. Lin, H.H. Ho, G.R. Pettit, E. Hamel, Antimitotic natural products combretastatin A-4 and combretastatin A-2: studies on the mechanism of their inhibition of the binding of colchicine to tubulin, Biochemistry 28 (1989) 6984–6991.

[19] Y.T. Ji, Y.N. Liu, Z.P. Liu, Tubulin colchicine binding site inhibitors as vascular disrupting agents in clinical developments, Curr. Med. Chem. 22 (2015) 1348–1360.

[20] P.O. Patil, A.G. Patil, R.A. Rane, P.C. Patil, P.K. Deshmukh, S.B. Bari, D.A. Patil, S.S. Naphade, Recent advancement in discovery and development of natural product combretastatin-inspired anticancer agents, Anticancer Agents Med. Chem. 15 (2015) 955–969.

[21] R. Kaur, G. Kaur, R.K. Gill, R. Soni, J. Bariwal, Recent developments in tubulin polymerization inhibitors: an overview, Eur. J. Med. Chem. 87 (2014) 89–124.

[22] R. Mikstacka, T. Stefański, J. Różański, Tubulin-interactive stilbene derivatives as anticancer agents, Cell Mol. Biol. Lett. 18 (2013) 368–397.

[23] Y. Shi, A phase I clinical trial assessing the safety and tolerability of combretastatin A4 phosphate injections, Anti-Cancer Drugs 25 (2014) 462–471.

[24] P. Nathan, M. Zweifel, A.R. Padhani, D.M. Koh, M. Ng, D.J. Collins, A. Harris, C. Carden, J. Smythe, N. Fisher, N.J. Taylor, J.J. Stirling, S.P. Lu, M.O. Leach, G.J.S. Rustin, I. Judson, Phase I trial of combretastatin A4 phosphate (CA4P) in combination with bevacizumab in patients with advanced cancer, Clin. Cancer Res. 18 (2012) 3428–3439.

[25] K. Ohsumi, R. Nakagawa, Y. Fukuda, T. Hatanaka, Y. Morinaga, Y. Nihei, K. Ohishi, Y. Suga, Y. Akiyama, T. Tsuji, Novel combretastatin analogues effective against murine solid tumors: design and structure-activity relationships, J. Med. Chem. 41 (1998) 3022–3032.

[26] M. Nishio, M. Satouchi, A. Horiike, Y. Orio, Y. Sunaga, E. Ecstein-Fraisse, T. Hida, Phase 1 study of ombrabulin in combination with docetaxel and cisplatin in Japanese patients with advanced tumors, Jpn. J. Clin. Oncol. 48 (2018) 322–328.

[27] S.N.A. Bukhari, G.B. Kumar, H.M. Revankar, H.L. Qin, Development of combretastatins as potent tubulin polymerization inhibitors, Bioorg. Chem. 72 (2017) 130–147.

[28] I.E.L.M. Kuppens, Current status of the art of new tubulin inhibitors in the clinic, Curr. Clin. Pharmacol. 1 (2006) 47–70.

[29] R. Romagnoli, P.G. Baraldi, M. Kimatrai Salvador, F. Prencipe, V. Bertolasi, M. Cancellieri, A. Brancale, E. Hamel, I. Castagliuolo, F. Consolaro, E. Porcu, G. Basso, G. Viola, Synthesis, antimitotic and antivascular activity of 1-(3',4',5'-trimethoxybenzoyl)-3-arylamino-5-amino-1,2,4-triazoles, J. Med. Chem. 57 (2014) 6795–6808.

[30] Among the twenty-two compounds with general structure 5, four of them (corresponding to derivatives 5a, 5e, 5f and 5h) were recently published by El-Sherief and co-workers as potential anticancer agents in this journal. H.A.M. El-Sherief, B.G.M. Youssif, S.N.A Bukhari, M. Abdel-Aziz, H.M. Abdel-Rahman. Novel 1,2,4-triazole derivatives as potential anticancer agents: Design, synthesis, molecular docking and mechanistic studies. Bioorg. Chem. 76 (2018) 314–325.

[31] K. Gaukroger, J.A. Hadfield, N.J. Lawrence, S. Nlan, A.T. McGown, Structural requirements for the interaction of combretastatins with tubulin: how important is the trimethoxy unit? Org. Biomol. Chem. 1 (2003) 3033–3037.

[32] A.S. Negi, Y. Gautam, S. Alam, D. Chanda, S. Luqman, J. Sarkar, F. Khan, R. Konwar, Natural antitubulin agents: importance of 3,4,5-trimethoxyphenyl fragment, Bioorg. Med. Chem. 23 (2015) 373–389.

[33] L. Hiser, A. Aggarwal, R. Young, A. Frankfurter, A. Spano, J.J. Correia, S. Lobert, Comparison of beta-tubulin mRNA and protein levels in 12 human cancer cell lines, Cell Motil. Cytoskeleton 63 (2006) 41–52.

[34] M.J. Pérez-Pérez, E.M. Priego, O. Bueno, M.S. Martins, M.D. Canela, S. Liekens, Blocking blood flow to solid tumors by destabilizing tubulin: an approach to targeting tumor growth, J. Med. Chem. 59 (2016) 8685–8711.

[35] A.E. Prota, F. Danel, F. Bachmann, K. Bargsten, R.M. Buey, J. Pohlmann, S. Reinelt, H. Lane, M.O. Steinmetz, The novel microtubule-destabilizing drug BAL27862 binds to the colchicine site of tubulin with distinct effects on microtubule organization, J. Mol. Biol. 426 (2014) 1848–1860.

[36] P. Barbier, A. Dorléans, F. Devred, L. Sanz, D. Allegro, C. Alfonso, M. Knossow, V. Peyrot, J.M. Andreu, Stathmin and interfacial microtubule inhibitors recognize a naturally curved conformation of tubulin dimers, J. Biol. Chem. 285 (2010) 31672–31681.

[37] Schrödinger Release 2017-1: Maestro, Schrödinger, LLC, New York, NY, 2017.

[38] Schrödinger Release 2017-1: Desmond Molecular Dynamics System, D. E. Shaw Research, New York, NY, 2017. Maestro-Desmond Interoperability Tools, Schrödinger, New York, NY, 2017.

[39] F. Adasme-Carreño, C. Muñoz-Guiterrez, J. Caballero, J.H. Alzate-Morales, Performance of the MM/GBSA scoring using a binding site hydrogen bond network-based frame selection: the protein kinase case, Phys. Chem. Chem. Phys. 16 (2014) 14047–14058.

[40] A.V. Dolzhenko, A.V. Dolzhenko, W.-K. Chui, Synthesis of 5,7-diamino[1,2,4]triazolo[1,2-a][1,3,5]triazines via annulation of 1,3,5-triazine ring onto 3(5)-amino-1,2,4-trizoles, Heterocycles 71 (2007) 429–436.

[41] A.V. Dolzhenko, G. Pastorin, A.V. Dolzhenko, W.K. Chui, An aqueous medium synthesis and tautomerism study of 3(5)-amino.1,2,4-triazoles, Tetrahedron Lett. 50 (2009) 2124–2128.

[42] Y. Naito, F. Akahoshi, S. Takeda, T. Okada, M. Kajii, H. Nishimura, M. Sugiura, C. Fukaya, Y. Kagitani, Synthesis and pharmacological activity of triazole derivatives inhibiting eosinophilia, J. Med. Chem. 39 (1996) 3019–3029.

[43] R. Romagnoli, P.G. Baraldi, C. Lopez-Cara, M. Kimatrai Salvador, D. Preti, M. Aghazadeh Tabrizi, M. Bassetto, A. Brancale, E. Hamel, I. Castagliuolo, R. Bortolozzi, G. Basso, G. Viola, Synthesis and biological evaluation of 2-alkoxycarbonyl-3-anilino benzo[b]thiophenes and thieno[2,3-b]pyridines as new potent anticancer agents, J. Med. Chem. 56 (2013) 2606–2618.

[44] E. Hamel, C.M. Lin, Separation of active tubulin and microtubule-associated proteins by ultracentrifugation and isolation of a component causing the formation of microtubule bundles, Biochemistry 23 (1984) 4173–4184.

[45] E. Hamel, Evaluation of antimitotic agents by quantitative comparisons of their effects on the polymerization of purified tubulin, Cell Biochem. Biophys. 38 (2003) 1–21.

[46] P. Verdier-Pinard, J.-Y. Lai, H.-D. Yoo, J. Yu, B. Marquez, D.G. Nagle, M. Nambu, J.D. White, J.R. Falck, W.H. Gerwick, B.W. Day, E. Hamel, Structure-activity analysis of the interaction of curacin A, the potent colchicine site antimitotic agent, with tubulin and effects of analogs on the growth of MCF-7 breast cancer cells, Mol. Pharmacol. 53 (1998) 62–67.